Article:
Colombo, M. orcid.org/0000-0002-4335-4250 and Fairweather, M. (2016) Accuracy of Eulerian–Eulerian, two-fluid CFD boiling models of subcooled boiling flows. International Journal of Heat and Mass Transfer, 103. pp. 28-44. ISSN 0017-9310

https://doi.org/10.1016/j.ijheatmasstransfer.2016.06.098

Accuracy of Eulerian – Eulerian, two-fluid CFD boiling models of subcooled boiling flows

M. Colombo* and M. Fairweather
School of Chemical and Process Engineering, University of Leeds, Leeds LS2 9JT, United Kingdom
E-mail addresses: M.Colombo@leeds.ac.uk, M.Fairweather@leeds.ac.uk

*Corresponding Author. Tel: +44 (0) 113 343 2351

Published paper https://doi.org/10.1016/j.ijheatmasstransfer.2016.06.098

ABSTRACT

Boiling flows are frequently found in industry and engineering due to the large amount of heat that can be transferred within such flows with minimum temperature differences. In the nuclear industry, boiling affects in different ways the operation of almost all water-cooled nuclear reactors. Recently, the use of Computational fluid dynamic (CFD) approaches to predict boiling flows is increasing and, in the nuclear area, CFD is being developed to solve thermal hydraulic safety issues such as establishing the critical heat flux, which is perhaps the major threat to the integrity of nuclear fuel rods. In this paper, the accuracy of an Eulerian – Eulerian, two-fluid CFD model is evaluated over a large database of subcooled boiling flows, avoiding the rather popular case-by-case tuning of descriptive models to a limited number of experiments. The model includes a Reynolds stress turbulence model, the method of moments-based S_γ population balance approach and a boiling model derived using the heat flux partitioning approach. The database covers a large range of conditions in subcooled boiling flows of water and refrigerants in vertical pipes and annular channels. Overall, a satisfactory predictive accuracy is achieved for some quantities of interest, such as the void fraction and the turbulence and liquid temperature fields, but results are less satisfactory in other areas, more specifically for the average bubble diameter and the mean velocity profiles close to the wall in annular channels. Agreement may be improved with advances in the treatment of large bubbles and bubble break-up and coalescence, as well as in improved modelling of the boiling region close to the wall, and more specifically the bubble departure diameter, the wall treatment and the contribution of bubbles to turbulence.

KEYWORDS: Subcooled boiling; computational fluid dynamics; two-fluid model; heat-flux partitioning; boiling model.

1 Introduction

In industry, boiling flows are often encountered because of the efficiency of heat transfer mechanisms under such conditions, which allow the transfer of significant amounts of heat with a limited amount of wall superheat, to the benefit of many engineering processes. In the nuclear industry, different types of boiling regimes are found in all water-cooled reactors, both in normal operation and during design-basis and beyond design-basis postulated accident transients. Boiling water reactors operate in the saturated boiling regime, and some degree of subcooled boiling is always experienced in pressurized water reactors during normal operation. Buoyancy-driven natural circulation loops and safety systems are also sometimes designed to operate within the boiling regime and, during loss of coolant accidents for example, boiling may occur due to the decrease in pressure and the reduced coolant inventory. For a reactor experiencing boiling conditions, the maximum amount of heat transferrable from the nuclear fuel to the coolant is referred to as the critical heat flux (CHF) and, when this is reached, the heat transfer deteriorates rapidly [1,2]. Recently, a significant portion of nuclear reactor thermal hydraulic analyses make use of multiphase computational fluid dynamic (CFD) models, and in particular of the Eulerian-Eulerian, averaged two-fluid formulation that is invariably used when addressing industrial-scale engineering problems. With respect to the simplistic models more commonly used in the nuclear industry, CFD may ultimately be able to describe phenomena in much greater detail, leading to the solution of selected nuclear reactor thermal hydraulic safety issues [3], including the prediction of CHF which, despite being perhaps the main threat to the integrity of nuclear fuel rods and despite long-term research efforts, has still resisted accurate modelling and understanding [4].

With the aim of predicting the boiling process, different wall boiling models have been incorporated in modern CFD codes. For two-fluid averaged models, these approaches are in the large majority based on the Rensselaer Polytechnic Institute (RPI) boiling model from Kurul and Podowski [5], where the heat flux from the wall is partitioned between the mechanisms responsible for the heat transfer process, these being single-phase convection, quenching and evaporation. In recent years, many authors have used more or less refined versions of the RPI boiling model to predict boiling flows [6-12]. After departure from the heated wall, the bubbles join the bulk of the flow and the size distribution of these bubbles, polydispersed in general, governs interphase exchanges of mass, momentum and energy. Therefore, in models of these flows, knowledge of the average diameter of the bubbles is required in many closure relations, and additional models have been used to predict the

74 average bubble diameter distribution. Initially, bubble size was derived from experimental
75 data or empirical correlations of subcooling in the liquid phase [5,13-16]. More recently,
76 bubble size distribution has been predicted by coupling different population balance
77 approaches to the two-fluid and the wall boiling models. Yao and Morel [6] derived source
78 terms for bubble coalescence, bubble break-up and phase change to be used in the volumetric
79 interfacial area transport equation. Yeoh and Tu [7] added wall nucleation and condensation
80 in the bulk flow to the multiple size group (MUSIG) model [17], which divides the bubble
81 diameter spectrum into a finite number of ranges to accommodate non-uniform bubble size
82 distributions. All these authors reported significant improvements over predictions based on
83 empirical correlations of subcooling of the liquid phase. More recently, Krepper et al. [10]
84 applied the inhomogeneous version of the MUSIG model, where each bubble size range is
85 allowed to have its own velocity, to the simulation of a subcooled boiling flow in a vertical
86 pipe. Morel and Lavieville [18] extended to boiling flows a method based on conservation of
87 the density S_γ of the moments of the bubble size distribution, which was assumed to obey to a
88 log-normal probability distribution. In their model, bubble break-up was not accounted for.
89 Bubble break-up was considered in the context of the S_γ model, initially proposed by Lo and
90 Rao [19] and Lo and Zhang [20], by Yun et al. [9], and more recently by Thakrar et al. [12],
91 to simulate boiling flows in a vertical pipe and in a vertical rectangular channel, respectively.
92 The boiling model calculates the amount of vapour generated at the wall and the
93 corresponding mass source is added to the near-wall computational cell. Here, in the large
94 majority of CFD codes, the boundary condition on the flow field is imposed using wall
95 functions. Wall functions for use in boiling flows have been developed by different authors
96 by including, in the single-phase law of the wall, an additional roughness due to the bubbles
97 attached at the wall [8,10,14].
98 Most of the boiling models have been tested against experimental measurements made in
99 subcooled boiling flows. The majority of these experiments were performed in circular cross-
100 section geometries, with water at low pressure [13] or refrigerant at moderate pressure [21-
101 23], because they scale to typical operating conditions found in water-cooled nuclear reactors.
102 At high pressure, the availability of data is more limited and the axial averaged void profiles
103 measured by Bartlomej and Chanturiya [24] and Bartolomej et al. [25] in upward pipe water
104 flows are perhaps the most extensively investigated case to date, in addition to the DEBORA
105 experiment [22], which, instead, focused on the boiling of refrigerant R12 at moderate
106 pressures. At high pressure, the measurements of Pierre and Bankoff [26] in a rectangular
107 channel have also received some attention [12].

In the majority of works to date, the boiling model is tested against a single experiment and, most frequently, a good predictive accuracy is demonstrated, but generally after calibration or tuning of some of the model parameters to the experiment under study [7,9,10,15]. Even if built in a mechanistic fashion, all the RPI-based models available at present are actually forced to rely on some empirical or semi-empirical closure relation, in particular for the evaporative heat transfer contribution, which requires knowledge of the active nucleation site density and the bubble departure diameter and frequency. The numerous empirical correlations available for this purpose were recently reviewed by Cheung et al. [27] and Thakrar et al. [28]. In general, poor predictive accuracy of these models has been found for subcooled boiling data over a wide range of mass and wall heat fluxes, and inlet subcooling, and no combination of correlations that provide a satisfactory overall accuracy has been identified. In the context of CFD, the most used correlations have been those of Lemmert and Chawla [29] and Hibiki and Ishii [30] for the active nucleation site density, of Tolubinsky and Kostanchuk [31] and Kocamustafaogullari [32] for the bubble departure diameter, and of Cole [33] for the bubble departure frequency [7,8,10,12,16]. However, attempts to assess the accuracy of these correlations for the conditions simulated are rather scarce, and no definitive information on the range of parameters over which any correlation is expected to provide a satisfactory accuracy, or simply outperform other correlations, is available. In view of these deficiencies, some authors have recently started to use more mechanistic formulations based on a balance of the forces acting on the growing bubble to calculate the bubble departure diameter [9,34].

In this paper, a large database of subcooled boiling flows in vertical channels examined experimentally over a wide range of operating conditions is assembled and predicted using a model solved using the STAR-CCM+ code. It has recently been noted [35,36] how it is necessary, to make progress in this field, to have models that are validated against numerous experiments, rather than on a case-by-case basis which only provides good agreement with a single experiment. This is particularly the case in the qualification of two-phase flow CFD codes for nuclear safety applications. In view of this, changes to any model should only be made if they are based on sound physical considerations, and following improvements to the overall performance of the model [35,36]. In this work, a priori selected closure models are applied to the whole database and the global accuracy of the model is evaluated (although some changes were necessary and will be explained throughout the text). The two-phase flow is described using an Eulerian-Eulerian two-fluid model, with boiling at the wall accounted for using the heat flux partitioning approach. The S_γ model, based on the moments of the

bubble size distribution, is used to predict the bubble diameter distribution, which governs the interfacial area density and therefore the interphase transfer processes. A multiphase Reynolds stress turbulence model is used, which, to the authors' knowledge, represents a level of closure in the context of boiling flows which has only been employed by Mimouni et al. [37,38] to predict the two-phase flow in a fuel bundle subjected to the influence of a mixing vane. Therefore, the impact of the use of a second-moment turbulence closure in subcooled boiling simulations is further investigated. In view of the large database adopted, the overall ability of multiphase CFD approaches to predict general boiling flows is evaluated, this being a necessary step if models of this kind are to be confidently applied to the prediction of the CHF. Areas that need further improvement are also identified and their impact on the global accuracy of the model is tested. Amongst others, the multiphase turbulence model and models for bubble coalescence and break-up, which are often one of the weakest aspects in the simulation of bubbly flows [36], are identified.

2 Model description

In a two-fluid Eulerian-Eulerian model, each phase is described by a set of averaged conservation equations, and the continuity, momentum and energy equations are solved for each phase. These, being discussed for adiabatic two-phase boiling flows in many previous publications [7,39,40] to which the interested reader may refer to, are not presented here. As a consequence of the averaging procedure, details of the interphase structure are lost and closure models are required for the mass, momentum and energy transfers at the interphase. These, and in particular the interphase momentum exchanges, have received much attention in recent years [41,42]. In this work, the drag model of Tomiyama et al. [43] is used, where the drag coefficient C_D is calculated from the bubble Reynolds and Eötvös numbers, *Re* and *Eo*:

$$C_D = max\left[\frac{24}{Re}(1 + 0.15Re^{0.687}), \frac{8Eo}{3(Eo + 4)}\right] \quad (1)$$

A lift force, perpendicular to the direction of motion, is experienced by bubbles moving in a shear flow [44] and this influences the radial void distribution in pipe and channel flows. Spherical bubbles are pushed towards the pipe wall whereas larger bubbles, which are more often oblate and ellipsoidal because of the inertia of the surrounding liquid, experience, after a critical value of the bubble diameter, a change of sign in the lift force and accumulate

towards the centre of the pipe [45]. In the literature, different correlations are available for the lift coefficient that also predict the change of sign with bubble diameter [45]. The wall force, in contrast, tends to keep bubbles away from a solid wall, and was modelled first by Antal et al. [46]. Lift and wall forces in adiabatic bubbly flows are fairly well established, although some uncertainties in their effective contributions, or in the actual accuracy of the available models, still exist [47,48]. Proof of the latter is found in the numerous different models that authors have used, even in the recent past. The use of lift and wall forces in boiling flows is much more uncertain and more general studies on the behaviour of bubbles near the heated wall are necessary. In view of these uncertainties, lift and wall forces were generally neglected. The turbulent dispersion force is modelled following Burns et al. [49], with a turbulent dispersion coefficient C_{TD} = 2.5 and a turbulent Prandtl number σ_α = 1.0 [49]:

$$F_{TD} = C_{TD}\frac{3}{4}\frac{C_D\alpha\rho_c|\boldsymbol{U}_r|}{\overline{d_B}}\frac{\nu_{t,c}}{\sigma_\alpha}\left[\frac{\nabla\alpha}{\alpha} - \frac{\nabla(1-\alpha)}{(1-\alpha)}\right] \tag{2}$$

2.1 Multiphase turbulence modelling

Turbulence is solved in the continuous phase only, with a Reynolds stress model (RSM) based on a multiphase formulation of the single-phase model due to Speziale, Sarkar and Gatsky (SSG) [50,51]:

$$\begin{aligned}\frac{\partial}{\partial t}\left((1-\alpha)\rho_c R_{ij}\right) + \frac{\partial}{\partial x_j}\left((1-\alpha)\rho_c U_{i,c} R_{ij}\right) \\ = \frac{\partial}{\partial x_j}\left[(1-\alpha)D_{ij}\right] + (1-\alpha)\left(P_{ij} + \Phi_{ij} - \varepsilon_{ij}\right) + (1-\alpha)S_{ij}^{BI}\end{aligned} \tag{3}$$

Here, P_{ij} is the turbulence production, the diffusion D_{ij} is modelled accordingly to Daly and Harlow [52] and the isotropic hypothesis is used for the turbulence energy dissipation rate ε_{ij}. The pressure-strain correlation Φ_{ij}, accounting for pressure fluctuations that redistribute the turbulence kinetic energy amongst the normal Reynolds stresses, is quadratically non-linear in the anisotropy tensor [50]. In the dispersed phase, turbulence was not resolved, but was instead directly related to the turbulence of the continuous phase by means of a response coefficient C_t, assumed equal to unity [53,54] following experimental evidence that suggests such a value is reached for void fractions as low as 6 % [55].

With respect to a single-phase flow, the generation of turbulence by bubbles can modify significantly the turbulence in the continuous phase [56-58]. To account for this contribution, bubble-induced source terms were included in the turbulence model assuming that all the energy lost by the bubbles to drag is converted into turbulence kinetic energy inside the bubble wakes [54,59,60]:

$$S_k^{BI} = K_{BI}\boldsymbol{F_d}\boldsymbol{U_r} \tag{4}$$

The corresponding turbulence energy dissipation rate source is equal to the turbulence kinetic energy source divided by the timescale of the bubble-induced turbulence, calculated from the velocity scale of the turbulence and the length scale of the bubbles [60]:

$$S_\varepsilon^{BI} = C_{\varepsilon,BI}\frac{S_k^{BI}}{\tau_{BI}} = 1.0\frac{k^{0.5}}{\overline{d_B}}S_k^{BI} \tag{5}$$

The mixed timescale, used in combination with the coefficient K_{BI} = 0.25, has been found to provide accurate predictions over a wide range of bubbly pipe flows [61]. The need for a bubble-induced turbulence contribution in bubbly flows has been demonstrated in many previous studies [48,54,60]. In contrast, less established is the use of these bubble-induced turbulence models in boiling flows and, therefore, this specific issue is further discussed in a specific section within the Results and discussion.

2.2 The S_γ model

Bubbles, after departure from the heated wall, experience evaporation and condensation in the bulk of the flow, and break-up and coalescence events that alter the bubble diameter distribution and affect the interphase mass, momentum and energy exchanges. The bubble diameter distribution is predicted with the S_γ model [19,20], where it is assumed to obey to a pre-defined log-normal probability distribution $P(d_B)$. From this, the density of the moments of the bubble size distribution M_γ may be derived:

$$S_\gamma = nM_\gamma = n\int_0^\infty d_B^\gamma P(d_B)\, d(d_B) \tag{6}$$

The zero[th] order moment is equal to the bubble number density n, whereas S_2 and S_3 are closely related to the interfacial area concentration and the void fraction:

$$S_0 = n;\ S_2 = n\int_0^\infty d_B^2 P(d_B)\, d(d_B) = \frac{a_i}{\pi};\ S_3 = n\int_0^\infty d_B^3 P(d_B)\, d(d_B) = \frac{6\alpha}{\pi} \tag{7}$$

Average diameters of different kinds of bubble are obtained by combining the moment densities, including, from S_2 and S_3, the Sauter-mean diameter (SMD), which is compared against experiments later:

$$d_{SM} = d_{32} = \frac{S_3}{S_2} = \frac{6\alpha}{a_i} \tag{8}$$

Additionally, the variance of the distribution is calculated from:

$$\sigma^2 = \ln\left(\frac{d_{32}}{d_{30}}\right) = \ln\left[\frac{(S_3/S_2)}{(S_3/S_0)^{1/3}}\right] \tag{9}$$

The two average diameters, d_{32} and d_{30}, are equal only for a monodispersed distribution. Since the void fraction is known from the two-fluid model, the solution of only two additional equations for S_0 and S_2 is sufficient to characterize the bubble size distribution. For each moment, a transport equation of the following type needs to be solved:

$$\frac{\partial S_\gamma}{\partial t} + \nabla\cdot\left(S_\gamma \boldsymbol{U}_v\right) = S_{br} + S_{cl} + S_m \tag{10}$$

The source terms account for the contributions of bubble break-up and coalescence, with the last being the source due to boiling at the wall and condensation/evaporation in the bulk of the flow:

$$S_m = N d_w^\gamma + \frac{2}{3}\frac{S_2 m_{lv}}{3\rho_v \alpha} \tag{11}$$

In this work, interactions induced by turbulence were assumed to be dominant and the only mechanism inducing break-up and coalescence events [6,20]. The source term for bubble break-up is expressed as:

$$S_{br} = \int_0^{\infty} K_{br} \Delta S_{\gamma}^{br} n P(d_B) d(d_B) \tag{12}$$

where K_{br} is the break-up rate, the reciprocal of the break-up time τ_{br}, and ΔS_{γ}^{br} is the change in S_{γ} due to a single break-up event, which, from conservation of volume, is:

$$\Delta S_{\gamma}^{br} = d_B^{\gamma} \left(N_f^{\frac{3-\gamma}{\gamma}} - 1 \right) \tag{13}$$

The number of daughter bubbles N_f was assumed equal to 2 [6,20,62]. The break-up timescale follows from the frequency of the second oscillation mode of a droplet [20]:

$$\tau_{br} = 2\pi k_{br} \sqrt{\frac{3\rho_d + 2\rho_c}{192\sigma} d_B^3} \tag{14}$$

with k_{br} = 0.2. Bubbles break when the Weber number is higher than a critical value We_{crit}, equal to 1.24 [6,48]:

$$d_{crit} = (1 + C_{\alpha}) \left(\frac{2\sigma We_{crit}}{\rho_c} \right)^{3/5} \varepsilon^{-2/5} \tag{15}$$

C_{α}, equal to 4.6, is a correction factor that accounts for nearby bubbles that disrupt the influence of the surrounding inertial forces. The general source term for bubble coalescence is:

$$S_{cl} = \int_0^{\infty} \int_0^{\infty} K_{cl}^{d,d\prime} \Delta S_{\gamma,cl}^{d,d\prime} n^2 P(d') d(d') P(d) d(d) \tag{16}$$

Here, $K_{cl}^{d,d\prime}$ is the coalescence rate between two bubbles with diameters d and d', and $\Delta S_{\gamma,cl}^{d,d\prime}$ is the change in S_{γ} due to a single coalescence event. Following [20], and to avoid excessive

computational cost, it is assumed, in the coalescence source term, that the bubble diameter has a uniform distribution with an equivalent mean diameter, taken equal to the SMD. Therefore, the change in S_γ due to a single coalescence event becomes:

$$\Delta S_{\gamma,cl}^{d,d'} = d_{SM}^{\gamma}\left(2^{\gamma/3} - 2\right) \tag{17}$$

From Yao and Morel [6], the number of coalescence events per unit volume and unit time is expressed as:

$$K_{cl}^{d,d'} n^2 = -C_1 \frac{\varepsilon^{1/3}\alpha^2}{d_{SM}^{11/3}} \frac{1}{g(\alpha) + C_2\sqrt{We/We_{crit}}} exp\left(-C_3\sqrt{We/We_{crit}}\right) \tag{18}$$

The first part of Eq. (18) represents the collision rate between the bubbles, whilst the exponential function describes the probability of coalescence following a collision event. The function $g(\alpha)$ accounts for the effect of the packing of the bubbles when the void fraction is higher than a certain value. From [6], $C_1 = 2.86$, $C_2 = 1.922$, $C_3 = 1.017$ and $We_{crit} = 1.24$.

2.3 Boiling model

When boiling occurs at a heated wall, different heat transfer mechanisms take place and these need to be modelled. In regions of the wall where no bubbles are growing, the heat is transferred to the liquid by single-phase convection. Otherwise, the heat is removed by the evaporation process and supports the growth of bubbles at the nucleation sites. Bubbles grow attached to the wall until, when certain conditions are reached, detachment occurs. Detachment of bubbles promotes additional mixing in the fluid phase and the recirculation of subcooled liquid which is brought into contact with the wall to fill the volume which was previously occupied by the detaching bubble. This mechanism accounts for a portion of the heat transferred from the wall, and is known as quenching. Finally, when a significant amount of vapour is present at the wall, liquid access to the wall may be restricted and a portion of the heat is transferred by convection to the vapour phase. Therefore, and following the RPI model of Kurul and Podowski [5], the total heat transferred from the wall is partitioned between these heat transfer mechanisms:

$$Q_w = \left(Q_l + Q_q + Q_{ev}\right)\left(1 - K_{dry}\right) + K_{dry}Q_v \tag{19}$$

K_{dry} is the fraction of the wall in contact with the vapour which becomes larger than zero when the void fraction is higher than a critical value, assumed equal to 0.9 [51]. The single-phase convective volumetric heat flux to the liquid phase is obtained from:

$$Q_l = (1 - A_b)\frac{\rho_l C_{p,l} u_{\tau,l}}{T_l^+}(T_w - T_l) \tag{20}$$

A_b is the fraction of the wall influenced by the evaporation process and T^+ a dimensionless temperature, which is calculated using the wall function approach [51]. In the same way, the convective volumetric heat flux to the vapour phase is known from:

$$Q_v = \frac{\rho_v C_{p,v} u_{\tau,v}}{T_v^+}(T_w - T_v) \tag{21}$$

The quenching volumetric heat flux, which accounts for the additional heat transfer to the cooler liquid that replaces a bubble detaching from the wall, is given by:

$$Q_q = h_q(T_w - T_l) \tag{22}$$

The quenching heat transfer coefficient is modelled accordingly to Del Valle and Kenning [63]:

$$h_q = 2A_b f\sqrt{\frac{\rho_l C_{p,l}\lambda_l t_w}{\pi}} \tag{23}$$

In the previous equation, t_w is the waiting time between the bubble departure and the nucleation of the next bubble:

$$t_w = \frac{0.8}{f} \tag{24}$$

In Eq. (22), and to avoid any dependency on the computational grid employed, the liquid temperature is evaluated at a constant y^+ of 250.

The evaporative volumetric heat flux is known from the number of bubbles that grow attached to the heated wall at the active nucleation sites. These bubbles grow until the forces that promote detachment overcome those that keep the bubble attached to the wall. Therefore, the evaporative heat flux is known from the number of active nucleation sites, the diameter of the bubbles at departure and the frequency of the bubble departure from the wall:

$$Q_{ev} = n' f \left(\frac{\pi d_w^3}{6} \right) \rho_v i_{lv} \tag{25}$$

In Eq. (25), closure relations are required for the nucleation site density, the bubble departure diameter and the bubble departure frequency. Most often, these have been obtained from empirical correlations. Only recently have more mechanistic formulations been introduced to calculate the bubble departure diameter [9,34]. In this work, two correlations for both the nucleation site density and for the bubble departure diameter are considered. Lemmert and Chawla [29] proposed correlating the nucleation site number density to the wall superheat:

$$n' = n_0 (T_w - T_{sat})^p \tag{26}$$

with n_0 = 12366.45 $m^{-2}K^{-1}$ and p = 1.805. More recently, it has become evident that, to have a model with a wide applicability, correlation to other parameters has to be taken into account, including properties of the heated surface such as the contact angle [30]. The more recent model from Hibiki and Ishii [30] is given by:

$$n' = n_0 \left[1 - exp\left(-\frac{\theta^2}{8\mu'^2} \right) \right] \left[exp\left(f' \frac{\lambda'}{R_c} \right) - 1 \right] \tag{27}$$

where $n_0 = 4.72 \times 10^5$ m^{-2}, $\mu' = 0.722$ rad and $\lambda' = 2.50 \times 10^{-6}$ m. θ is the contact angle, f' a function of $\rho^+ = \log(\Delta\rho / \rho_v)$ and R_c is equal to:

$$R_c = \frac{2\sigma[1 + \rho_v/\rho_l]/p}{exp\left[i_{lv}(T_v - T_{sat})/R_g T_v T_{sat} \right] - 1} \tag{28}$$

Tolubinsky and Kostanchuk [31] correlated the bubble departure diameter to the liquid subcooling:

$$d_w = d_0 exp[-(T_{sat} - T_l)/\Delta T_0] \quad (29)$$

Here, d_0 = 0.0006 m and ΔT_0 = 45 K. Kocamustafaogullari [32] developed a model for the bubble departure diameter based on a balance between gravity and surface tension forces. The model, with the addition of the dependency on a density ratio, was developed to account for the effect of the system pressure:

$$d_w = d_l \theta \left(\frac{\sigma}{g\Delta\rho}\right)^{0.5} \left(\frac{\Delta\rho}{\rho_v}\right)^{0.9} \quad (30)$$

where $d_l = 1.5126 \times 10^{-3}$ m rad^{-1} and $\theta = 0.722$ rad for water systems. The bubble departure frequency is calculated from Cole [33]:

$$f = \sqrt{\frac{4}{3}\frac{g(\rho_l - \rho_v)}{d_w \rho_l}} \quad (31)$$

The fraction of the wall affected by the evaporation process is known from [5]:

$$A_b = 2.0 \frac{\pi d_w^2}{4} n' \quad (32)$$

Finally, in the bulk of the fluid, the liquid side heat transfer coefficient at the interphase is calculated using the Ranz and Marshall [64] correlation:

$$h_l = \frac{\lambda_l}{d_B}\left(2 + 0.6 Re^{1/2} Pr^{1/3}\right) \quad (33)$$

The overall model, implemented in the STAR-CCM+ CFD code [51], is solved in a two-dimensional axisymmetric geometry. At the inlet, fully-developed single-phase liquid velocity, turbulence and temperature are imposed, together with an imposed pressure at the outlet and the no-slip condition, and an imposed heat flux, at the wall. Strict convergence of residuals was ensured, together with a mass balance error always lower than 0.01 % for both phases. A mesh sensitivity study demonstrated that grid-independent solutions were achieved

with an equidistant structured mesh with the first grid point placed at a minimum wall distance of $y^+ = 30$, which is the lower limit for the use of wall functions.

3 Experimental data

Confidence in the predictions of CFD codes relies on extensive validation of their results against relevant experimental data. In this regard, it is important that models provide accurate predictions over many experiments, with parameter variations as wide as possible. Therefore, a database was built from 20 experiments from 5 different sources: Bartlomej and Chanturiya [24], Bartolomej et al. [25], Roy et al. [21], the DEBORA experiment [22] and Lee et al. [13]. The database, which is summarized in Table 1, includes measurements in vertical pipes and annular channels of subcooled boiling flows of water, Freon-12 and refrigerant R-113, and covers the ranges 0.101 – 6.89 MPa for the pressure, 477 – 2981 kg $m^{-2}s^{-1}$ for the mass flux, 58.2 – 1200 kW m^{-2} for the heat flux and 11.5 – 63 °C for the inlet subcooling.

The DEBORA [22] flow loop consisted of a 19.2 mm inner diameter vertical pipe, heated for a length of 3.5 m and operated with Freon-12 (R-12). Given the inherent difficulties of measuring the flow boiling of water at high pressure, and temperature, Freon-12 guaranteed more favourable experimental conditions, while maintaining values of dimensionless groups such as the Reynolds and the Weber number, and the density ratio, consistent with typical operating conditions of pressurized water reactors. Measurements were taken in the ranges 1.46 – 3.01 MPa for the pressure, 1000 – 3000 kg $m^{-2}s^{-1}$ for the mass flux and 58 – 135 kW m^{-2} for the heat flux, and a significant range of liquid subcooling. Void fraction and vapour velocity profiles at the end of the test section were measured with an optical probe technique, from which radial profiles of the interfacial area concentration and the SMD were determined. Thermocouples were used to measure the liquid temperature radial profile and the wall temperature at selected axial locations.

Batolomej and Chanturiya [24], and Bartolomej et al. [25], investigated the subcooled boiling of water in vertical pipes of inlet diameter D = 0.0154 m and 0.012 m, and length L = 2 m and 1.4 m, respectively. Average void fractions were measured at different axial locations at pressures up to 15 MPa, mass fluxes up to 2000 kg $m^{-2}s^{-1}$ and heat fluxes up to 2.2 MW m^{-2}. For this study, five cases were selected from these experiments at pressures up to 6.89 MPa, mass fluxes up to 1500 kg $m^{-2}s^{-2}$ and heat fluxes up to 1.2 MW m^{-2} (Table 1).

Roy et al. [21] tested the subcooled boiling of refrigerant R-113 in a vertical annulus of 3.66 m in length, 0.0158 m in inlet diameter and 0.0381 m in outlet diameter. A laser Doppler

velocimetry system allowed measurement of the velocity field and the turbulent fluctuations, with an optical probe used to obtain the void fraction and the bubble diameter. The liquid and vapour temperatures were measured with micro-thermocouples. Measurements were taken at 0.269 MPa and in the ranges 565 – 785 kg $m^{-2}s^{-1}$ for the mass flux, 79.4 – 125.9 kW m^{-2} for the heat flux and 42.7 – 50.2 °C for the inlet temperature. In a slightly different annular channel, 2.376 m in length, 0.019 m in inlet diameter and 0.0375 m in outlet diameter, Lee et al. [13] investigated the subcooled flow boiling of water at nearly atmospheric pressure, and 474 – 1061 kg $m^{-2}s^{-1}$ for the mass flux, 115 – 300 kW m^{-2} for the heat flux and 11.5 – 21.3 °C for the inlet subcooling. Liquid velocity radial profiles were measured with a Pitot tube, and vapour velocity and void fraction radial profiles with a two-conductivity probe method.

None of the previous experiments provides a complete characterization of the flow, which is a shortcoming of most of the experimental data available to date. Limited measurements of the bubble diameter are available from Roy et al. [21] and, therefore, the DEBORA experiment is the only one that provides radial profiles of the average bubble diameter. However, in the DEBORA experiment, liquid velocity profiles and liquid turbulence profiles were not measured. Turbulence profiles, in particular, are only available from Roy et al. [21]. Temperatures were measured in the DEBORA and the Roy et al. [21] experiments, but not by Lee et al. [13], which also did not provide any information on liquid turbulence and bubble diameter. Finally, in Bartolomej and Chanturiya [24] and Bartolomej et al. [25], and since these experiments were undertaken at higher pressures and some decades ago, only the average void fraction at different axial locations was measured. Even so, these experiments are one of the few to give measurements at high pressure. The use of a large database therefore overcame the limitation of each individual dataset, allowing validation of the model for all physical quantities of interest. It is important to note, however, the necessity for more detailed and comprehensive experimental data sets in order to improve our ability to predict these kinds of flows, since, as will be seen in the following section, the parameters of interest interact with each other in a rather complex and non-linear way.

Table 1. Summary of the experimental conditions included in the validation database.

Data	Source	p [MPa]	p_r [-]	G [kg m^{-2}s^{-1}]	q" [kW m^{-2}]	T_{in} [°C]	Fluid	Geometry
deb1	Garnier et al. [22]	2.62	0.63	1996	73.9	68.5	R12	P
deb2	Garnier et al. [22]	2.62	0.63	1985	73.9	70.5	R12	P
deb3	Garnier et al. [22]	1.46	0.35	2023	76.3	39.7	R12	P
deb4	Garnier et al. [22]	1.46	0.35	2028	76.2	34.9	R12	P
deb5	Garnier et al. [22]	2.62	0.63	2981	109.4	69.2	R12	P
deb6	Garnier et al. [22]	3.01	0.73	1007	58.2	64.6	R12	P
roy1	Roy et al. [21]	0.269	0.08	565	79.4	42.7	R113	A
roy2	Roy et al. [21]	0.269	0.08	785	95.0	50.2	R113	A
roy3	Roy et al. [21]	0.269	0.08	785	125.9	50.2	R113	A
lee1	Lee et al. [13]	atm	0.005	478	152.8	80.8	W	A
lee2	Lee et al. [13]	atm	0.005	477	114.8	88.5	W	A
lee3	Lee et al. [13]	atm	0.005	718	232.6	78.8	W	A
lee4	Lee et al. [13]	atm	0.005	714	197.2	86.2	W	A
lee5	Lee et al. [13]	atm	0.005	1061	300.0	81.9	W	A
lee6	Lee et al. [13]	atm	0.005	1047	251.2	86.6	W	A
bar1	Bartolomej and Chanturiya [24]	1.5	0.07	900	380	138.3	W	P
bar2	Bartolomej and Chanturiya [24]	4.5	0.20	900	570	197.4	W	P
bar3	Bartolomej et al. [25]	6.89	0.31	1500	1200	221.9	W	P
bar4	Bartolomej et al. [25]	6.89	0.31	1500	800	245.9	W	P
bar5	Bartolomej et al. [25]	6.89	0.31	1000	800	229.9	W	P

atm = atmospheric; W = water; P = pipe; A = annular channel.

4 Results and discussion

4.1 Coalescence source

Before simulating the whole database, some model parameters had to be selected, starting with the coalescence source, calculated from Yao and Morel [6]. In a previous work, a critical Weber number We_{crit} = 0.10 in the coalescence efficiency allowed good agreement to be obtained for different air-water bubbly flows in vertical pipes [65]. This agreement was achieved in combination with the assumption of negligible bubble break-up, which is expected to be even lower in boiling flows due to the lower expected bubble diameter. In bubbly flow experiments, therefore, bubbles are usually injected with a diameter of the order of a few millimetres. In contrast, during boiling, bubbles may detach from the wall with a diameter up to one or two orders of magnitude smaller.

Yao and Morel [6] proposed a value of 1.24 for We_{crit}, rather higher than the value of 0.1 adopted in [65]. These two values are compared for the deb1 and deb2 experiments (see Table 1) in Figure 1. In the plots, profiles of the SMD and the void fraction are shown as a function of the normalized radial distance, with the centre of the pipe located at r/R = 0.0 and the wall at r/R = 1.0. As expected, We_{crit} has a significant impact on the SMD radial profile. More specifically, We_{crit} = 0.10 leads to a large underestimation of the SMD, probably as a consequence of weak bubble coalescence in the flow. With We_{crit} = 1.24, the SMD is still under predicted in deb1 (Figure 1a), although the agreement is improved. For deb2, the

results are more in line with the experimental measurements (Figure 1c). Relative to the SMD, other variables are less affected by the amount of coalescence, this being the case in Figure 1 for the void fraction radial profiles (Figure 1b and Figure 1d). To provide a further evaluation, experiment bar5 was also simulated and the axial distribution of the cross-sectional averaged void fraction is shown in Figure 2. In this case, the difference between the simulation results is more marked, with lower coalescence in the flow causing a lower average void fraction, probably as a consequence of the higher condensation. The condensation heat transfer coefficient is indeed inversely proportional to the bubble diameter. In view of these results, We_{crit} = 1.24 was selected for the following simulations.

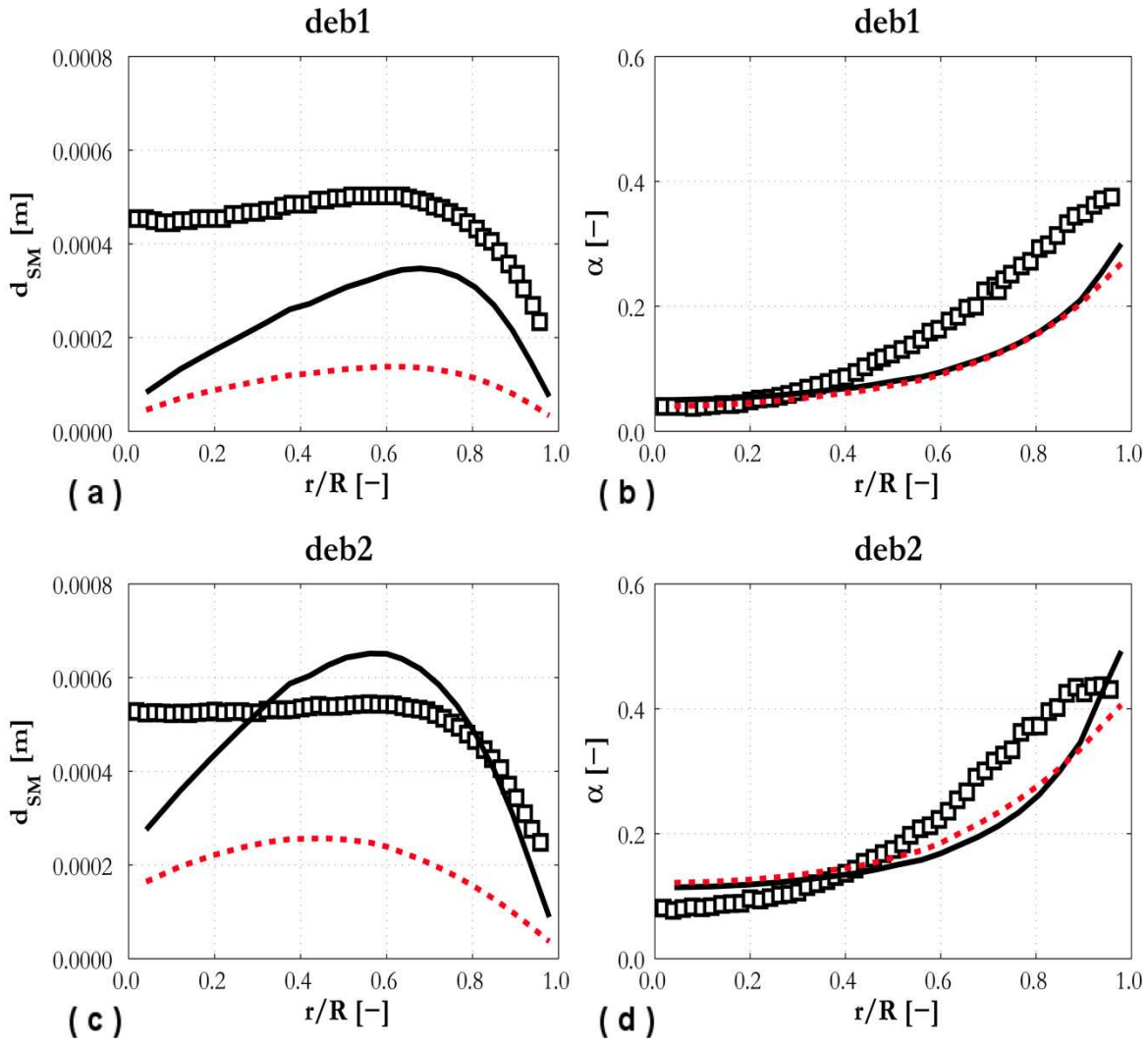

Figure 1. SMD and void fraction radial profiles compared against experiments deb1 (a,b) and deb2 (c,d) and for different values of We_{crit} in the coalescence model: (—) 1.24; (---) 0.1.

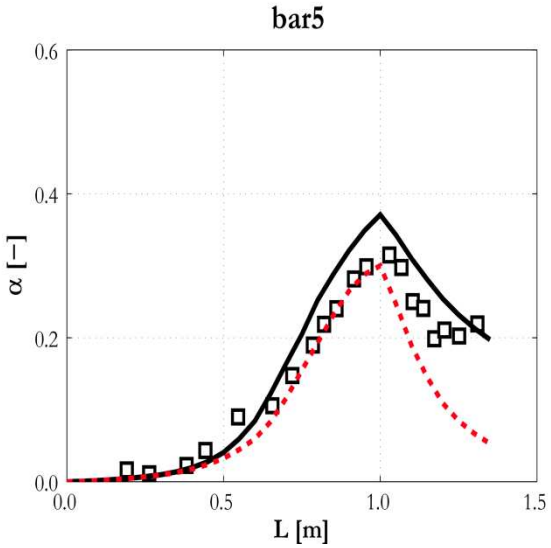

Figure 2. Average void fraction axial development compared against experiment bar5 and for different values of We_{crit} in the coalescence model: (—) 1.24; (---) 0.1.

4.2 Bubble departure diameter

In preliminary simulations, it was found impossible to use, in the boiling model, the same set of closure relations to address the entire database, in particular for the active nucleation site density and the bubble departure diameter. For the nucleation site density, the Hibiki and Ishii model [30] was maintained for the entire database because it accounts for the effect of more parameters. Due to the fact that the database extends from atmospheric pressure up to 6.89 MPa, the Kocamustafaogullari model [32] was initially considered for the bubble departure diameter, this being derived over the range $0.0067 < p < 14.18$ MPa. In contrast, the Tolubinsky and Kostanchuck [31] correlation was derived for $0.1 < p < 1.013$ MPa and $0.08 < U_l < 0.20$ m s^{-1} and has a pressure insensitive formulation, with the bubble departure diameter being only a function of the bulk subcooling. Unfortunately, using the Kocamustafaogullari correlation [32], reliable results were not obtained for the Roy et al. [21] data and the experiments of Bartolomej and co-authors [24,25]. An example is provided in Figure 3, which shows predictions of the void distribution given by this correlation for the bar2 (Figure 3b) and the bar4 (Figure 3d) experiments and compares these with the results obtained using the Tolubinsky and Kostanchuk [31] correlation (Figure 3a and Figure 3c, respectively). In the figure, $r/R = 0.0$ corresponds to the pipe axis and $r/R = 1.0$ to the pipe wall. For bar2, at 4.5 MPa, Kocamustafaogullari [32] predicts a void fraction that is comparable with that from Tolubinsky and Kostanchuk [31]. At higher pressure (bar4, 6.89 MPa), however, the void fraction predicted with Kocamustafaogullari [32] is almost negligible, except for a very thin portion of the wall region. Therefore, due to the negligible

521 evaporation predicted in some of the experiments, for the data of Bartolomej and Chanturiya
522 [24], Bartolomej et al. [25] and Roy et al. [21], the Tolubinsky and Kostanchuk [31]
523 correlation was used.
524 To investigate the subject further, some bubble departure diameter data selected from the
525 literature was tested against the Kocamustafaogullari model [32]. These data were taken from
526 Unal et al. [66] for water at high pressure, and from Klausner et al. [67] and Zeng et al. [68]
527 who used refrigerant R113, as employed by Roy et al. [21], at atmospheric pressure.
528 Percentage relative errors between predictions and data are shown in Figure 4. In general, the
529 bubble departure diameter is under predicted. More specifically, 50 – 75 % smaller diameters
530 are found for refrigerant R113 and, for water, the departure diameter is overestimated at low
531 pressure, but under predicted by up to 100% at high pressure. Overall, the relative percentage
532 errors are rather high, therefore the model cannot be considered reliable over a wide range of
533 conditions.
534 In line with the approach of the paper, it would have been desirable to maintain the
535 Tolubinsky and Kostanchuk [31] correlation for the whole database. However, this
536 correlation is also not entirely reliable even given its range of validity, as it was found that
537 unrealistically large bubbles were predicted by it for some of the Lee et al. [13] and the
538 DEBORA [22] experiments at low pressure, which prevented convergence of the simulations.
539 Therefore, for these two databases, the Kocamustafaogullari [32] correlation was used.
540
541

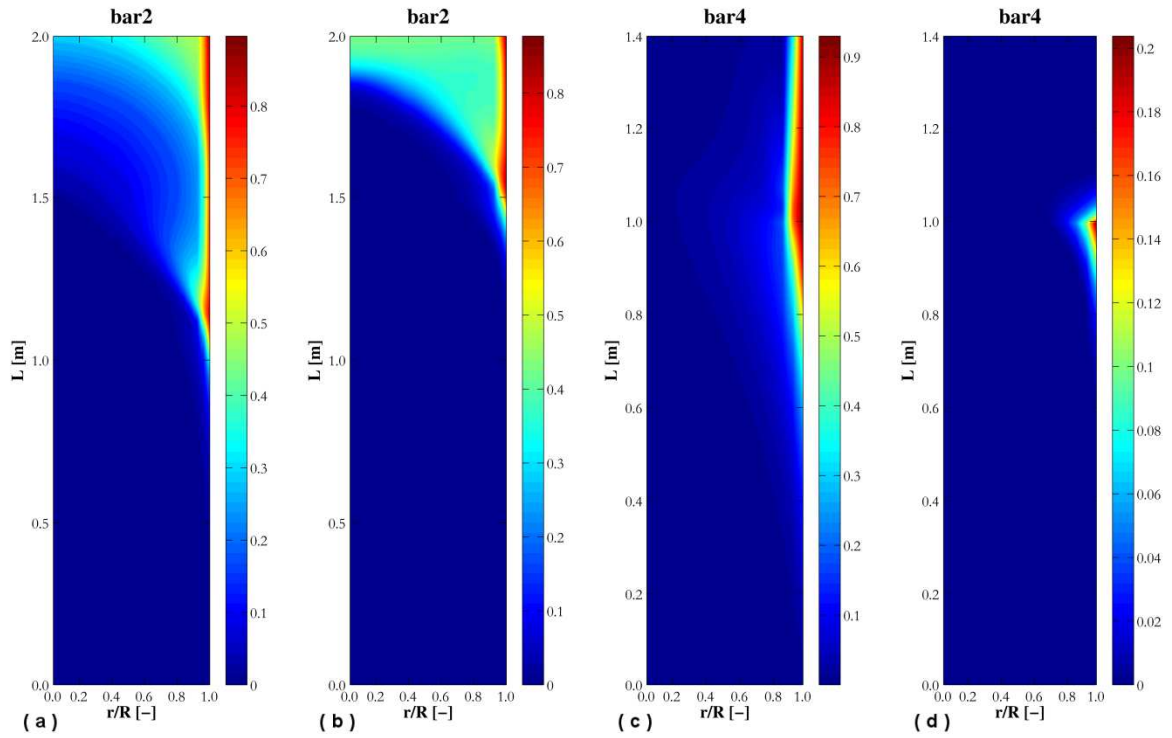

Figure 3. Void fraction radial distribution along the pipe for bar2 and bar4 experiments: (a,c) Tolubinsky and Kostanchuk [31] bubble departure diameter correlation; (b,d) Kocamustafaogullari [32] bubble departure diameter correlation.

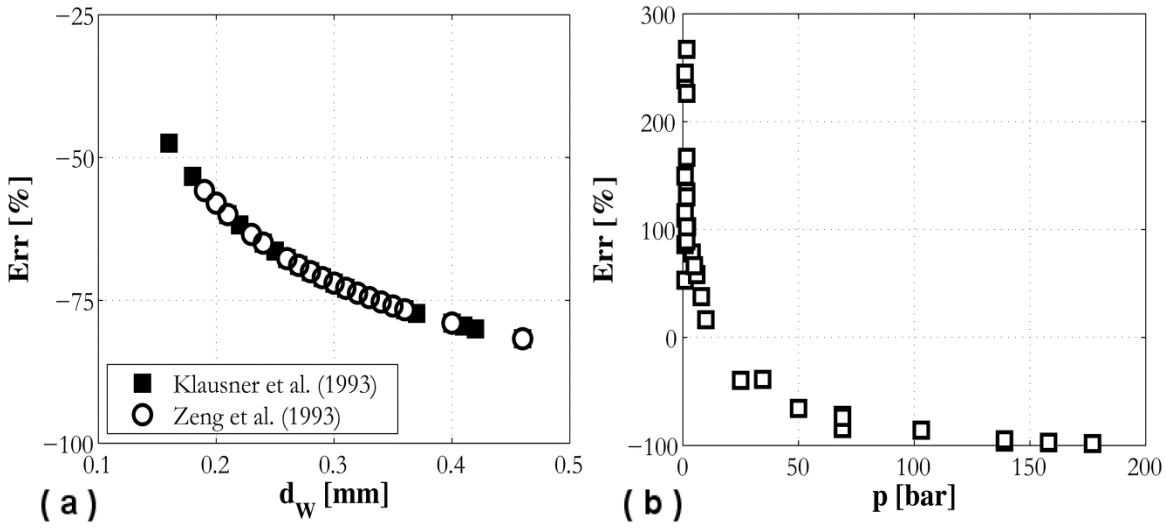

Figure 4. Relative percentage error for the Kocamustafaogullari [32] bubble departure diameter correlation compared against: (a) Klausner et al. [67] and Zeng et al. [68] for refrigerant R113; (b) Unal et al. [66] for water at different pressures.

554 **4.3 Comparison with the entire database**
555
556 After the preliminary selection of some of the model parameters, the overall model was
557 applied to the whole database without further modification. Comparisons for the DEBORA
558 experiments are presented in Figure 5 and Figure 6, and in Figure 7 for Roy et al. [21], in
559 Figure 8 for Lee et al. [13] and in Figure 9 for Batolomej and Chanturiya [24] and Bartolomej
560 et al. [25]. In these, and subsequent figures, symbols are used for experimental data and lines
561 for model predictions. In annular channels (Figure 7 and Figure 8), the radial position is non-
562 dimensionalized with the distance between the outer and inner radius and, therefore, in the
563 plots $(r - R_i) / (R_o - R_i) = 0.0$ identifies the inner wall, whereas $(r - R_i) / (R_o - R_i) = 1.0$
564 corresponds to the outer wall. Only the inner wall is heated in both the Roy et al. [14] and the
565 Lee et al. [13] experiments. In the following, discussion of the results is presented for each
566 physical quantity predicted.
567

568 ***4.3.1 Void fraction***
569 Even if the specific quantitative accuracy depends on the particular experiment, the void
570 fraction profile is generally predicted with reasonable accuracy. More specifically, the
571 accuracy is satisfactory for the DEBORA experiment (Figure 5 and Figure 6), but with the
572 exception of deb6 (Figure 6c) where the void profile is significantly under predicted. Also, an
573 over predicted void peak at the heated wall was obtained for deb4 (Figure 6a). For deb3, it
574 must be remarked that the void fraction profile (Figure 5j) is core-peaked and the bubble
575 diameter (Figure 5k) higher than in all the other experiments. It is known from the literature
576 that larger bubbles assume ellipsoidal shapes, being deformed by the inertia of the
577 surrounding liquid, and are pushed towards the centre of the pipe by a negative lift force [45].
578 In this experiment, bubbles may have been large enough to trigger the change of sign in the
579 lift force and, even if wall-peaked void profiles were predicted neglecting the lift
580 contribution, a negative lift was necessary to predict the void profile. In Figure 7, void
581 fraction profiles are well predicted for Roy et al. [21], the only discrepancy being a minor
582 underestimation in the case of roy3. In contrast, the void fraction tends to be underestimated
583 in the experiments of Lee et al. [13] (Figure 8). More specifically, the predicted void fraction
584 is in agreement with experiment or over predicted near the wall, whereas it is underestimated
585 in the remainder of the pipe. The best results are obtained at the lowest mass flux (lee1 in
586 Figure 8a and lee2 in Figure 8c), and the largest errors in lee5 (Figure 8i). Lastly, in the
587 Bartolomej and co-authors' experiments [24,25], only the averaged axial void distribution

588 was available and this is well predicted for bar1 and bar2 (Figure 9a), apart from a divergence
589 at around 1.25 m in bar2. Reasonable agreement is found for the Bartolomej et al. [25]
590 experiments in Figure 9b, despite the slight over prediction in bar3 and bar5.
591

592 ***4.3.2 Sauter-mean diameter***

593 Measurements of the SMD were available for the DEBORA experiments only. Overall, the
594 model under predicts the experiments, in particular near the centre of the pipe, although
595 reasonable agreement is achieved for experiments deb2 (Figure 5g) and deb3 (Figure 5k),
596 whereas the under prediction is particularly large in deb6 (Figure 6e). In more detail, the
597 SMD is underestimated close to the heated wall and, after a partial improvement in the first
598 region away from the wall, predictions decrease significantly towards the pipe axis. In
599 contrast, the experimental profiles tend to remain nearly flat towards the centre of the pipe. In
600 deb3 (Figure 5k), the SMD increases towards the pipe centre, most likely as a consequence of
601 the core-peaked void fraction profile in this experiment, a trend that is also predicted by the
602 simulation. Overall, the significant discrepancies with the experiments may be due to a
603 number of different factors, the individual impact of which is difficult to quantify. Certainly,
604 the interphase heat transfer coefficient and the models for coalescence and break-up may play
605 a role that needs to be investigated further. In addition, the underestimation of the SMD in the
606 wall region suggests a significant impact of the bubble departure diameter correlation. This,
607 in conjunction with the unreliability of each bubble departure correlation over a wide range of
608 conditions, discussed in Section 4.2, demonstrates how the development of more advanced,
609 mechanistic formulations of the bubble departure diameter is a priority for further research.
610

611 ***4.3.3 Liquid temperature***

612 Liquid temperature profiles were measured by Roy et al. [21] and in the DEBORA
613 experiments. Overall, predictions are in good agreement with data. For the DEBORA
614 experiments, the flat temperature profile for deb2 (Figure 5h) and deb3 (Figure 5l) indicates a
615 flow close to saturation that may have helped to limit the underestimation of the SMD for
616 these experiments (Figure 5g and Figure 5k). deb1 (Figure 5d), instead, shows a slightly
617 higher degree of subcooling near the axis. The Roy et al. [21] experiments (Figure 7d, Figure
618 7h and Figure 7l), which exhibit a higher degree of subcooling away from the wall, are also

well predicted, despite the temperature being slightly over estimated close to the wall and under estimated near the axis.

4.3.4 Velocity profiles

Liquid and vapour average velocities were measured by Roy et al. [21] and Lee et al. [13], whereas only the average vapour velocity profile is available for the DEBORA experiments. The vapour velocity profile is very well predicted for deb3 (Figure 5i), although for deb1 (Figure 5a) and deb2 (Figure 5e), the profile remains flat near the pipe centre, probably as a consequence of the lower value of the SMD in this region. However, predictions may be considered satisfactory for these pipe flows. On the other hand, the predicted accuracy is unsatisfactory in the annular channels of Roy et al. [21] and Lee et al. [13]. More specifically, both predicted velocity profiles show a peak at the wall that is in contrast found away from the wall in the experiments (Figure 7b, Figure 7f, Figure 7j, Figure 8b, Figure 8d, Figure 8f, Figure 8h, Figure 8j and Figure 8l). This phenomenon is even more evident in the vapour velocity profiles. Away from the wall, in particular for Roy et al. [21], the velocity profiles are more in agreement with the experiments. The peak away from the wall is explained due to the presence, in this region, of larger bubbles that flow with a higher relative velocity. In Lee et al. [13], probably as a consequence of the atmospheric pressure that promotes the growth of even larger bubbles, these peaks are sometimes found in the "unheated half" of the channel. In the simulations, however, the SMD peaks at the wall and the model is unable to correctly account for the presence of the larger bubbles, with this inability also contributing to the low SMD values and the flat velocity profiles in the centre of the channel predicted in deb1 (Figure 5a) and deb2 (Figure 5e).

4.3.5 Turbulence

Turbulence was only measured by Roy et al. [21] and the streamwise and radial r.m.s. of the liquid velocity fluctuations are shown in Figure 7c, Figure 7g and Figure 7k. Overall, turbulence is well predicted except for the under predicted streamwise r.m.s. in roy1 (Figure 7c). Also, the anisotropy of the turbulence field is reasonably well predicted by the Reynolds stress turbulence model.

One of the advantages of building such a large database is the opportunity it affords to test any model for all the variables of interest. However, and in view of the present results that

show the strengths of the model in some areas but weaknesses in others, measurements of all the variables of interest in the same experiment are essential to further progress in the modelling of boiling flows.

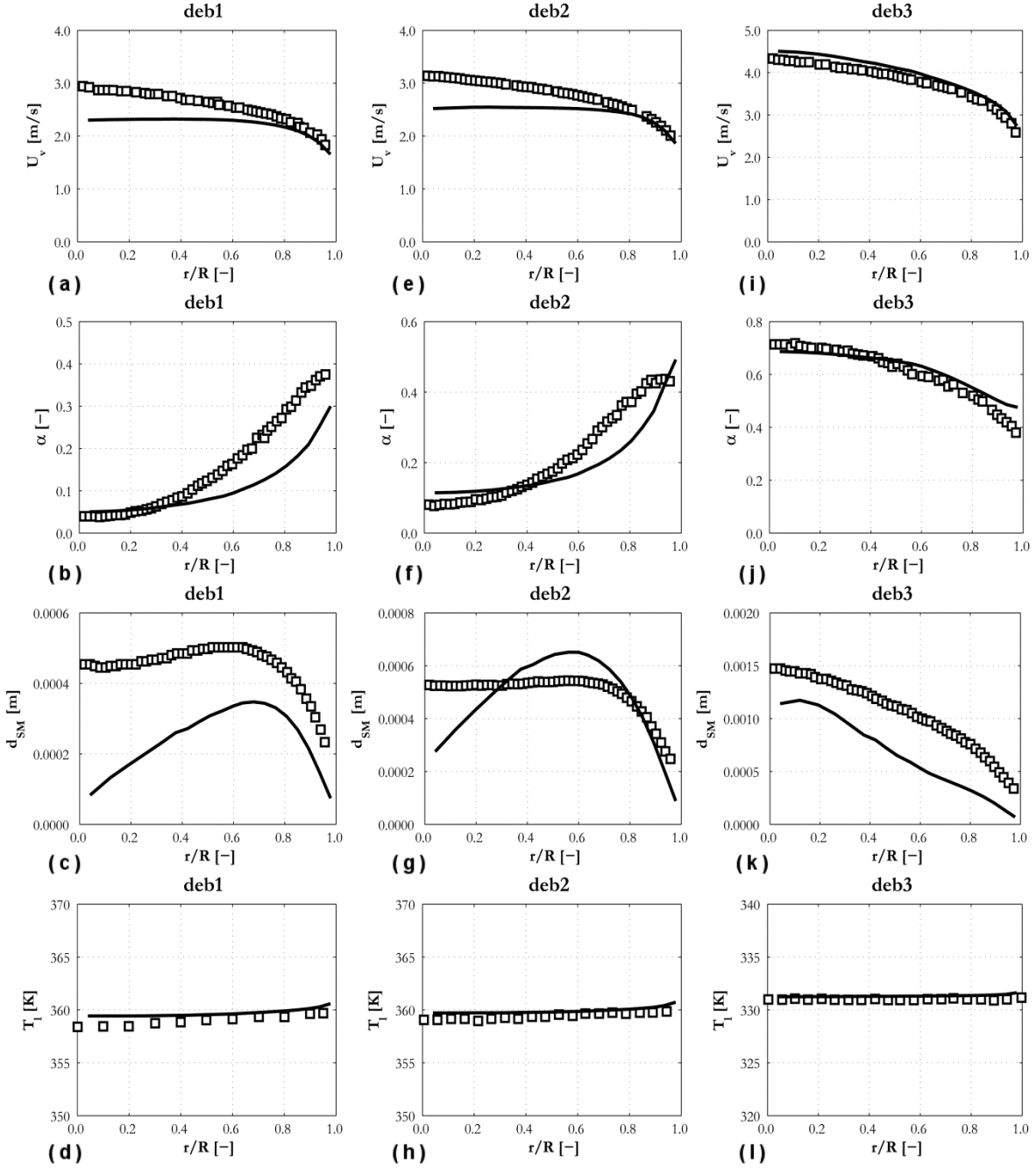

Figure 5. Average vapour velocity, void fraction, SMD and liquid temperature radial profiles compared against the DEBORA experiments: (a-d) deb1; (e-h) deb2; (i-l) deb3.

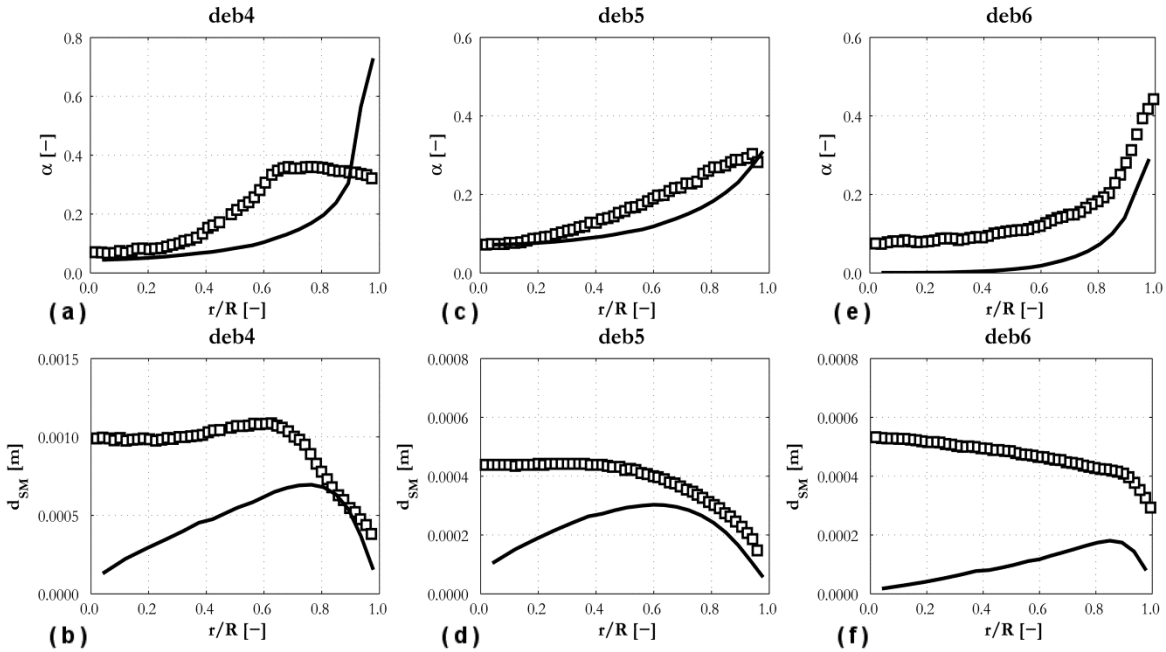

659
660 Figure 6. Void fraction and SMD radial profiles compared against the DEBORA
661 experiments: (a-b) deb4; (c-d) deb5; (e-f) deb6.
662

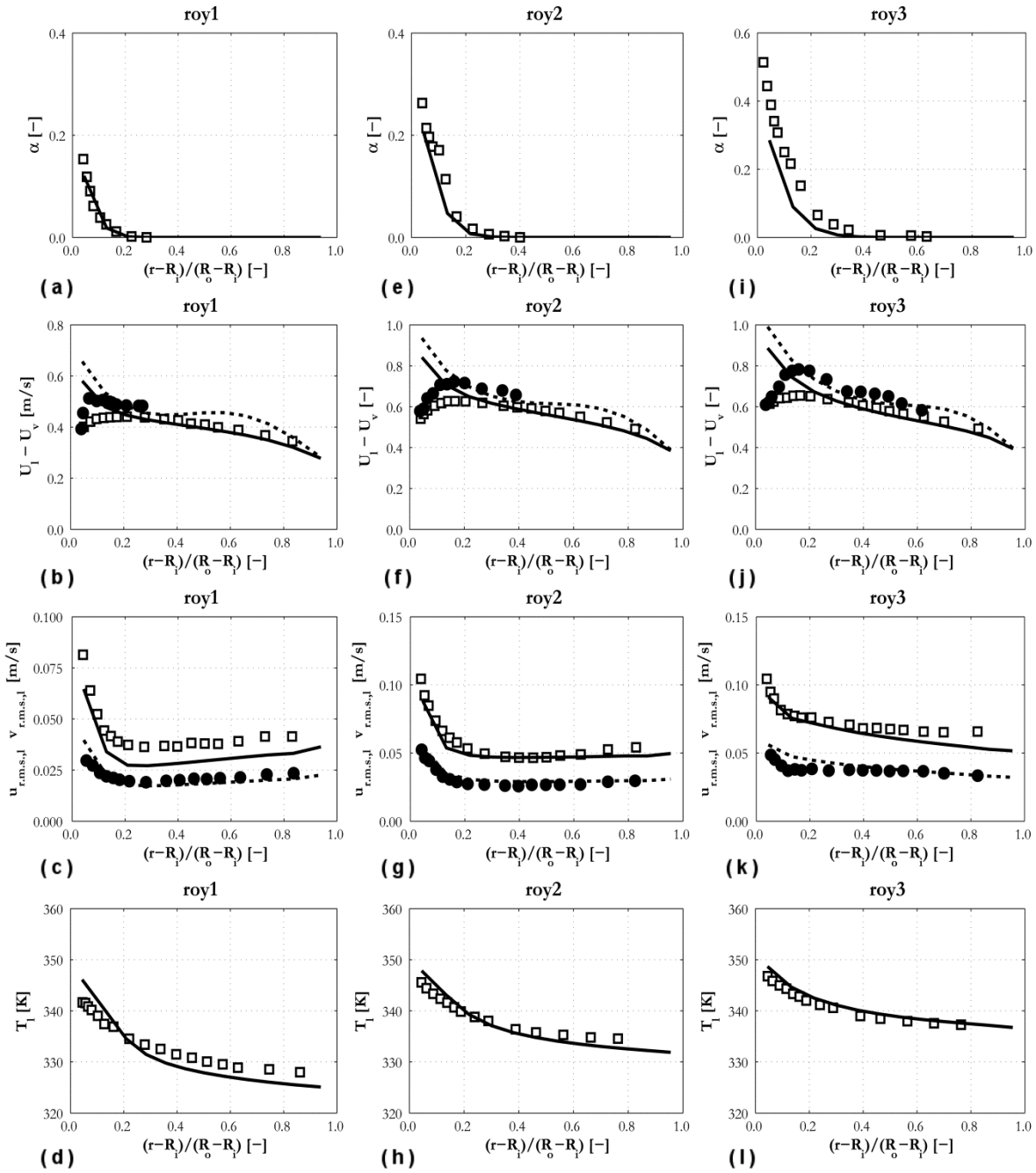

Figure 7. Void fraction, liquid (—,□) and vapour (---,●) average velocity, streamwise (—,□) and radial (---,●) r.m.s. of liquid velocity fluctuations and liquid temperature radial profiles compared against Roy et al. [21]: (a-d) roy1; (e-h) roy2; (i-l) roy3.

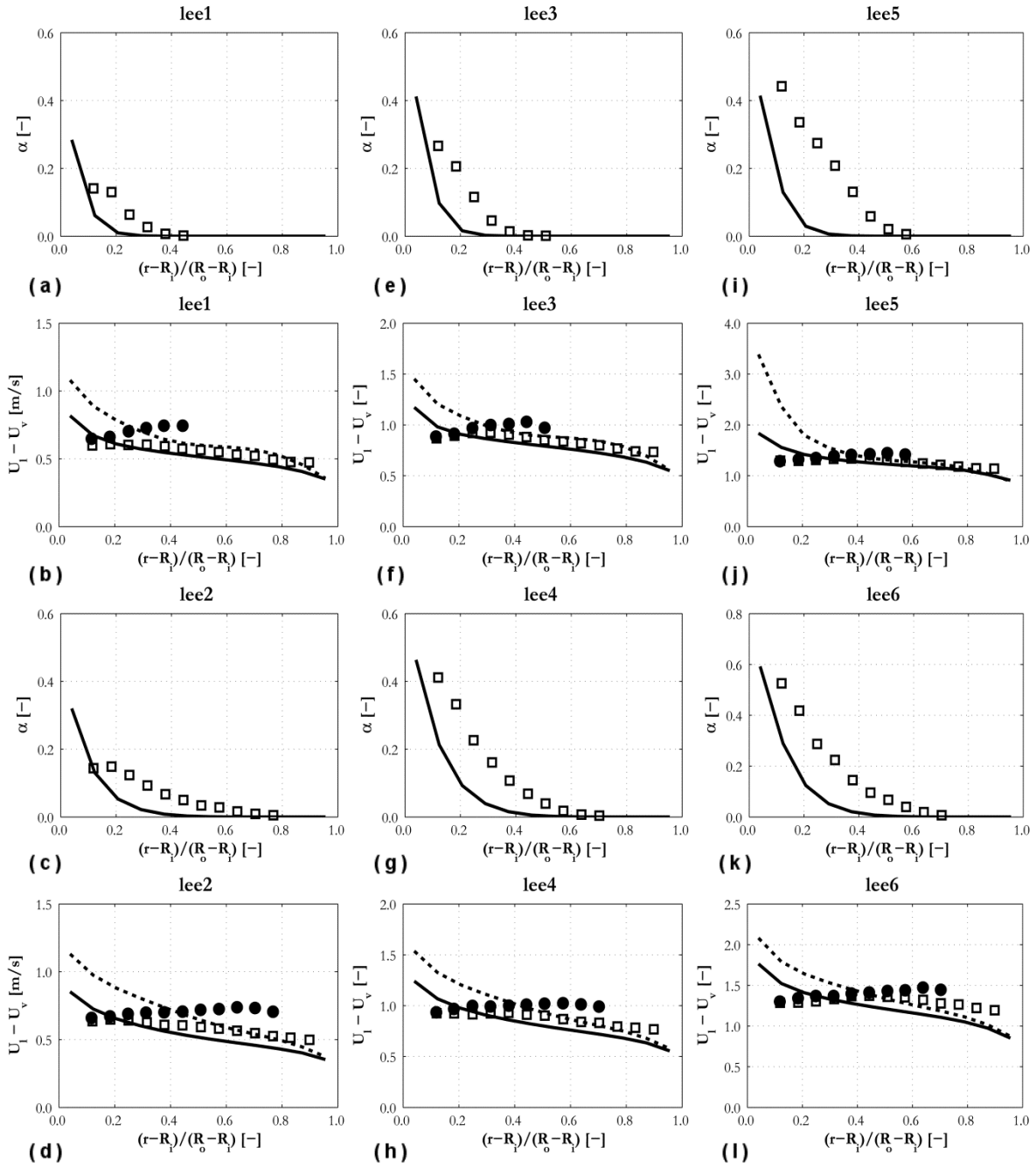

Figure 8. Void fraction and liquid (—,□) and vapour (---,●) average velocity radial profiles compared against Lee et al. [13]: (a,b) lee1; (c,d) lee2; (e,f) lee3; (g,h) lee4; (i,j) lee5; (k,l) lee6.

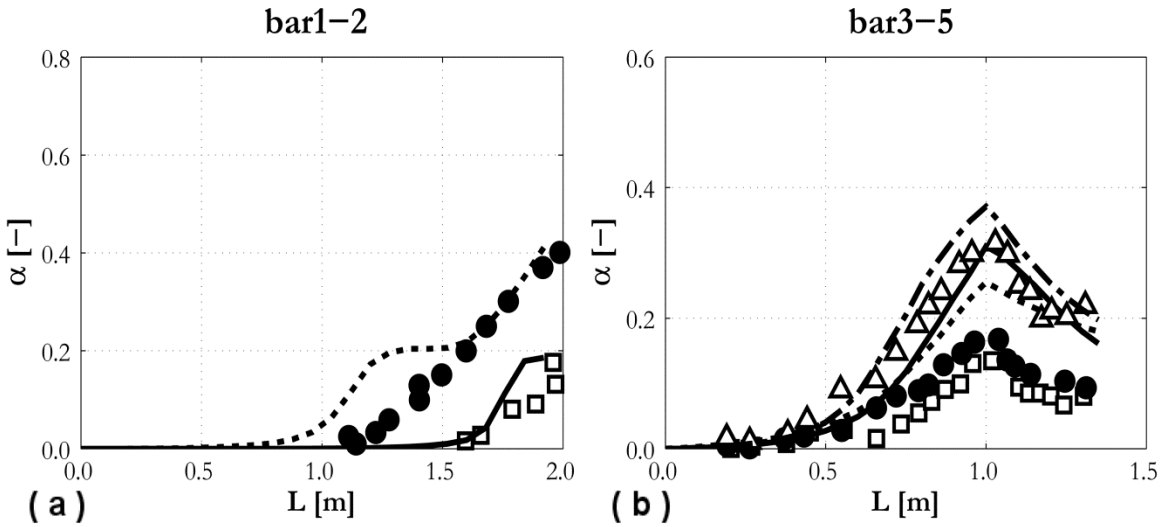

Figure 9. Average void fraction axial development compared against: (a) Bartolomej and Chanturiya [24]; (b) Bartolomej et al. [25]. (a): (—,□) bar1; (---,●) bar2. (b): (—,□) bar3; (---,●) bar4; (-·-,Δ) bar5.

4.4 Near-wall treatment

In the previous section, the most significant deviations from experiments were found for the average velocity profiles in the near-wall region of annular channels. In the last computational cell close to the wall, the velocity boundary condition is imposed through the use of wall functions, with the standard single-phase wall function having been used in the simulations. Some authors [8,9,69] have demonstrated how predictions in the near-wall region can be improved with the adoption of a simple wall roughness model, similar to those used in turbulent flows over rough surfaces, but with the equivalent roughness equal to the bubble departure diameter. To the authors' knowledge, such a modification has yet to be tested with an RSM turbulence model. In a first set of simulations with the RSM, it was found difficult to reach convergence and handle the rather high wall roughness values (equal to the bubble departure diameter). Therefore, the wall roughness model was tested using a k-ε formulation. The results are reported in Figure 10 for experiments roy2, roy3 and lee2, and, for the k-ε model with the standard wall function, these show the same features discussed for the RSM, i.e. liquid and vapour average velocity profiles show the same peak at the wall and rather high values with respect to the experiments.

For the lower void fraction cases (roy2 and lee2), agreement for the liquid velocity improves and the profile peaks at a certain distance from the wall with inclusion of the wall roughness model (Figure 10b and Figure 10j). These improvements are limited to the roy2 experiment

for the vapour velocity profile (Figure 10c). In the highest void fraction experiment (roy3), the improvement is also marginal for the liquid velocity (Figure 10f and Figure 10g). In roy2 and roy3, the wall roughness model also produces an increase in the void fraction (Figure 10a and Figure 10e), although this remains unchanged in lee2 (Figure 10i).

Overall, the introduction of the wall roughness model is seen to improve the predictions, although the improvements noted are not significant in all cases examined. In addition to further development of the wall model and its extension for use with RSM, it also seems necessary, based on the discussion in Section 4.3.4, to better account for the behaviour of larger bubbles, extending to boiling flows recently developed population balance models that account for their behaviour separately [10,65].

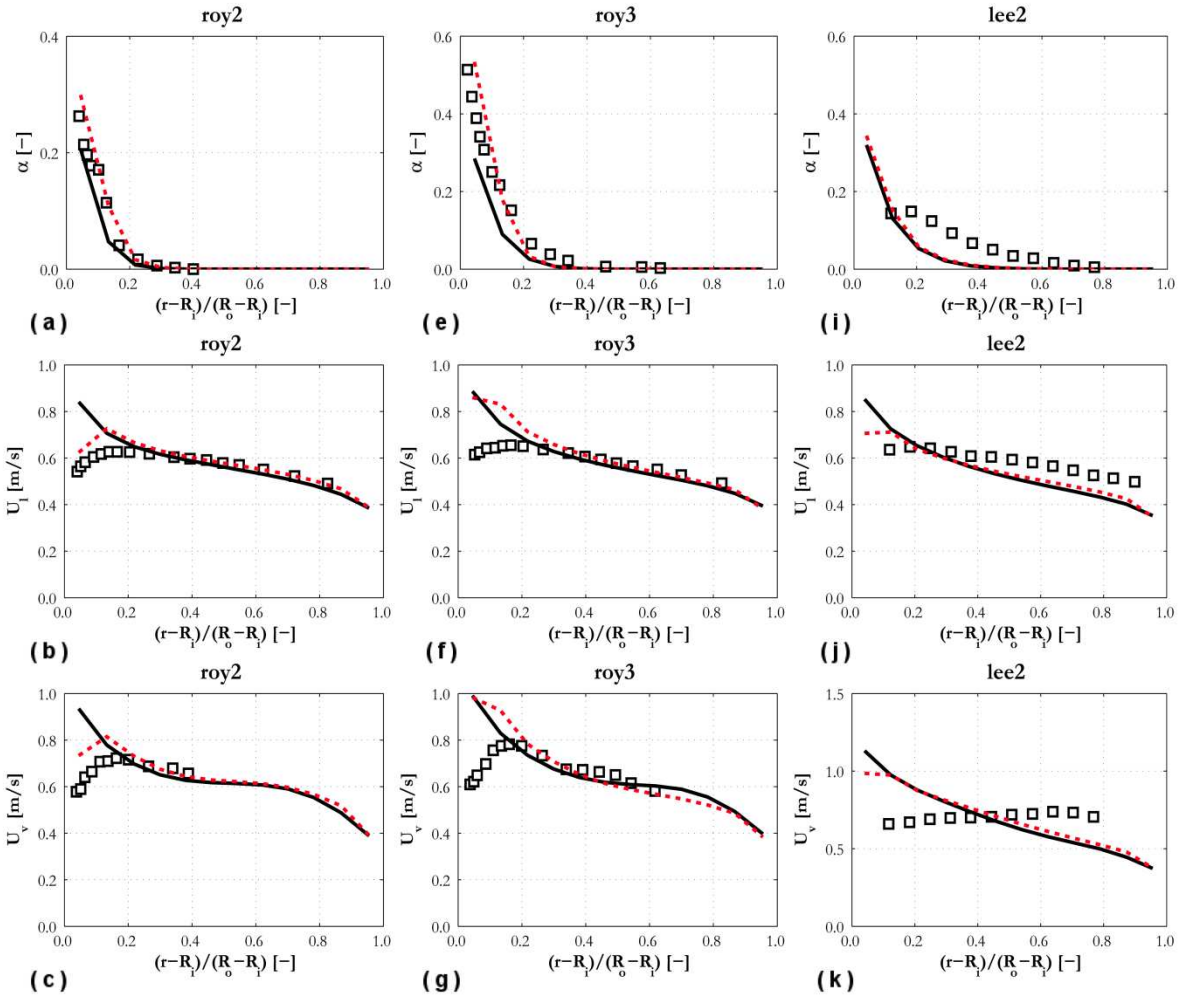

Figure 10. Void fraction and average liquid and vapour velocity radial profiles compared against Roy et al. [21] and Lee et al. [13]: (a-c) roy1; (e-g) roy2; (i-k) roy3. (—) standard wall function; (---) wall roughness model [8].

4.5 Bubble-induced turbulence

It has been established how, in bubbly flows, the bubbles contribute to the turbulence of the continuous phase and this contribution must be accounted for in the turbulence model [48,54,60]. Many studies have been conducted on the subject, but only a few of them have focused on boiling flows, and, therefore, the impact of the bubble contribution on the turbulence is much more uncertain in these flows. In Section 4.3.5, the bubble-induced contribution was neglected. Nevertheless, turbulence in the continuous phase was well predicted, even if measurements were available only for Roy et al. [21] (Figure 7c, Figure 7g and Figure 7k). This may suggest that bubble-induced turbulence is less important with respect to adiabatic bubbly flows even if it must be noticed that, in Roy et al. [21], the void fraction is very low or zero in the majority of the channel (Figure 7a, Figure 7e and Figure 7i). Also, in the regions of high void fraction close to the wall, this influence is further complicated with respect to adiabatic bubbly flows due to the detachment into the bulk fluid of bubbles growing on the heated wall.

The roy1 and roy3 calculations were repeated with the bubble-induced turbulence model (Eq. (4) and Eq. (5)) and the results are shown in Figure 11. In roy1, the r.m.s. values are changed only in the region very close to the wall (Figure 11c), where the velocity fluctuations are now overestimated. The same effect is obtained for roy3 and for a larger portion of the pipe section (Figure 11f). Therefore, the model accuracy is generally worsened with inclusion of the bubble-induced turbulence model. Void fraction (Figure 11a and Figure 11d) and average velocity (Figure 11b and Figure 11e) predictions are also increased relative to those without the bubble-induced turbulence contribution. The findings are, however, complicated by the fact that, due to the peak in the velocity profiles, the shear-induced turbulence close to the wall may also be overestimated and this may be the reason for the overestimation of turbulence levels when the bubble-induced contribution is accounted for. More studies are necessary on this subject, but, since bubbles detachment occurs in the first computational cell close to the wall, and in view of the results from the previous section on the wall treatment, it is suggested that the problem needs to be approached globally, addressing jointly in the same model the velocity boundary condition and the generation of turbulence close to the wall, as well as the contribution from the bubbles in this region.

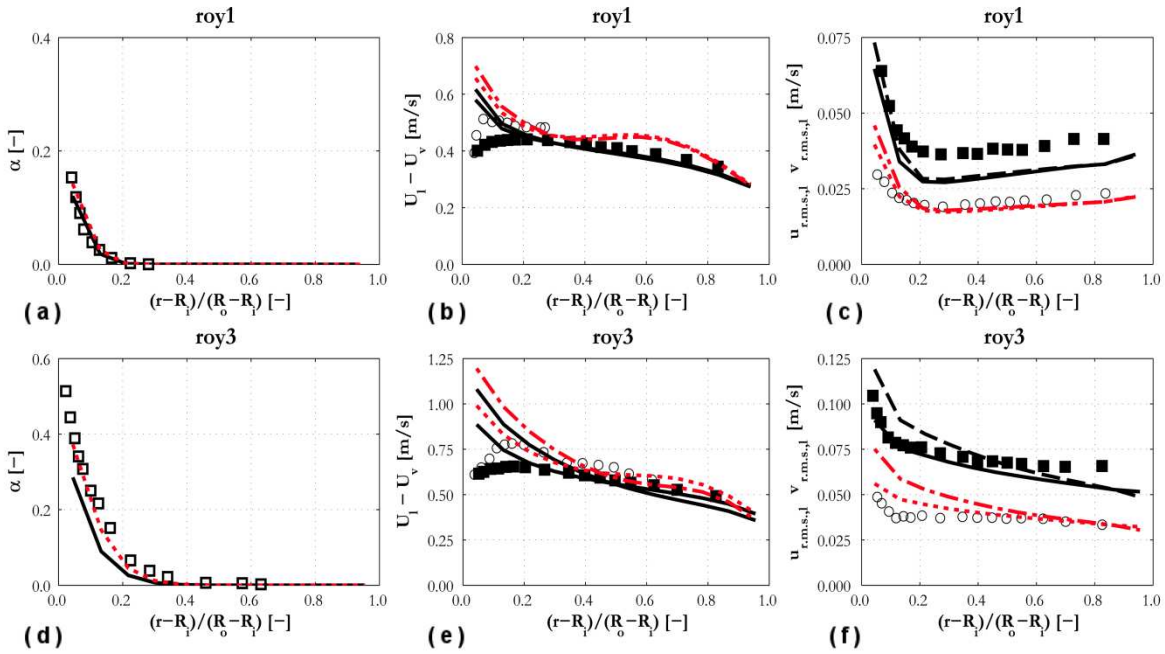

Figure 11 Void fraction, liquid (□,—,––) and vapour (○,---,-··-) average velocity and streamwise (□,—,––) and radial (○,---,-··-) r.m.s. of the liquid velocity fluctuations radial profiles compared against Roy et al. [21]: (a-c) roy1; (d-f) roy3. (—,---) without bubble induced turbulence model; (––,-··-) with bubble induced turbulence model.

5 Conclusions

An Eulerian-Eulerian two-fluid CFD model, including a Reynolds stress turbulence model, the method of moments-based S_γ population balance approach and a boiling model derived from the RPI heat flux partitioning approach, was used to predict a large database of subcooled boiling flows. The database includes 20 experiments of subcooled boiling flows of water and refrigerants in vertical pipes and annular channels, and covers a wide range of conditions.

Overall, the model confirms the potential of CFD to provide detailed predictions of boiling flows and rather good agreement with data was found in some areas, but others still require significant improvements in model accuracy. At the present time, the general applicability of the model is not entirely satisfactory. Even if built in a mechanistic fashion, numerous empirical closure relations are required, not only for wall boiling, but also for the population balance and turbulence models. This clearly limits the overall model's general applicability and, therefore, the development of more mechanistic closures is highly desirable. A good example is provided by the bubble departure diameter that cannot be predicted with accuracy over extended ranges of conditions by the presently available correlations. The development

of physically-based, more accurate closure models is challenging and may only be achieved with an increase in our knowledge of mechanisms that are as yet not completely understood, such as the growth and departure of bubbles, but also their breakup and coalescence and the interaction of turbulence with bubbles near the wall, amongst others.

The results show how studies such as the one described, which focused on a large database, can profitably be used to integrate detailed analyses based on more limited amounts of data. In the latter, major developments of specific sub-models can be derived and tested, but these developments can only be accepted if they improve the general accuracy of models when tested against large sets of data. The disparity observed between individual experiments suggests that it is risky to judge the accuracy of any CFD model on the basis of a limited number of comparisons with data.

Quantitatively, the predictive accuracy is satisfactory for the void fraction, except for a limited number of cases, with the turbulence and liquid temperature fields also well predicted. In contrast, the average bubble diameter, quantified by the SMD, tends to be underestimated, sometimes significantly, in particular near the axis of the flows, with velocity profiles also over predicted near the heated wall of annular channels, where they exhibit a peak that is instead found away from the wall in the experiments.

Despite the inaccuracy of some predictions, the satisfactory results achieved in some areas encourage further research:

- No correlation for the bubble departure diameter was found appropriate for the entire database and the under prediction of the departure diameter was identified as a possible source of error in the average bubble diameter predictions. The use of more mechanistic formulations, already adopted by a limited number of researchers, represents a way forward in this regard.
- Modelling of bubble break-up and coalescence needs to be improved, with related improvements in population balance modelling also required. More specifically, the ability to account for larger bubbles moving towards the flow centre, already available for adiabatic flows, may improve the prediction of velocity profiles in both pipes and channels.
- Velocity predictions near the wall were improved using a wall roughness model, but further development is required, in particular in the context of RSM.
- Bubble-induced turbulence was demonstrated to be less relevant with respect to adiabatic flows and the use of a specific model provided inconsistent results. A more

advanced modelling approach seems necessary near the wall, but it should be addressed together with the wall treatment.

Acknowledgements

The authors gratefully acknowledge the financial support of the EPSRC under grant EP/K007777/1, Thermal Hydraulics for Boiling and Passive Systems, part of the UK-India Civil Nuclear Collaboration.

Nomenclature

A_b	fraction of the wall affected by the evaporation process [m^{-1}]
a_i	interfacial area concentration [m^2 m^{-3}]
C_D	drag coefficient [-]
C_p	specific thermal capacity at constant pressure [J kg^{-1} K^{-1}]
D	diameter [m]
d_B	bubble diameter [m]
d_{crit}	critical bubble diameter [m]
d_{SM}	Sauter mean diameter [m]
d_w	bubble departure diameter [m]
Eo	bubble Eotvos number $Eo = g\,(\rho_l - \rho_v)\,d_B^2 / \sigma$ [-]
F_d	drag force [N m^{-3}]
F_{TD}	turbulent dispersion force [N m^{-3}]
f	frequency of bubble departure [s^{-1}]
G	mass flux [kg $m^{-2}s^{-1}$]
g	gravitational acceleration [m s^{-2}]
h_q	quenching heat transfer coefficient [W $m^{-3}K^{-1}$]
i_{lv}	latent heat of vaporization [J kg^{-1}]
K_{br}	break-up rate [s^{-1}]
$K_{cl}^{d,d'}$	coalescence rate [s^{-1}]
K_{dry}	fraction of the heated wall in contact with the vapour phase [-]
k	turbulence kinetic energy [m^2s^{-2}]
L	pipe/channel length [m]
M_γ	γ^{th} moment of the bubble diameter distribution [m^γ]
m_{lv}	interphase mass transfer [kg $m^{-3}s^{-1}$]
N	bubble generation rate per unit volume [bubbles $m^{-3}s^{-1}$]

840	N_f	number of daughter bubbles [-]
841	n	bubble number density [bubbles m^{-3}]
842	n'	nucleation site density [m^{-2}]
843	$P(d_B)$	bubble diameter probability distribution [-]
844	Pr	Prandtl number $Pr = C_p \mu / k$ [-]
845	p	pressure [Pa]
846	p_r	reduced pressure p/p_{crit} [-]
847	Q_{ev}	evaporative volumetric heat flux [W m^{-3}]
848	Q_l	liquid phase convective volumetric heat flux [W m^{-3}]
849	Q_q	quenching volumetric heat flux [W m^{-3}]
850	Q_v	vapour phase convective volumetric heat flux [W m^{-3}]
851	Q_w	total wall volumetric heat flux [W m^{-3}]
852	q''	heat flux [W $m^{-2}K^{-1}$]
853	R	radius [m]
854	R_g	gas constant [J $mol^{-1}K^{-1}$]
855	R_{ij}	Reynolds stress [m^2s^{-2}]
856	r	radial coordinate [m]
857	Re	bubble Reynolds number $Re = \rho_l U_r d_B / \mu_l$ [-]
858	S_{br}	source of S_γ due to bubble break-up [m^γ $m^{-3}s^{-1}$]
859	S_{cl}	source of S_γ due to bubble coalescence [m^γ $m^{-3}s^{-1}$]
860	S_m	source of S_γ due to boiling and evaporation [m^γ $m^{-3}s^{-1}$]
861	S_k^{BI}	bubble-induced turbulence kinetic energy source [kg m s^{-3}]
862	S_ε^{BI}	bubble-induced turbulence energy dissipation rate source [kg m s^{-4}]
863	S_γ	density of the γ^{th} moment of the bubble diameter distribution [m^γ m^{-3}]
864	ΔS_γ^{br}	change in S_γ due to a single break-up event [m^γ]
865	$\Delta S_{\gamma,cl}^{d,d\prime}$	change in S_γ due to a single coalescence event [m^γ]
866	T	temperature [°C]
867	T^+	dimensionless temperature [-]
868	t	time [s]
869	t_w	waiting time for bubble departure [s]
870	$\boldsymbol{U}$	velocity [m s^{-1}]
871	$u_{r.m.s.}$	streamwise r.m.s. of the velocity fluctuations [m s^{-1}]
872	$v_{r.m.s.}$	radial r.m.s. of the velocity fluctuations [m s^{-1}]

u_τ	shear velocity [m s^{-1}]
We	Weber number $We = \rho_l \, u \, d_B / \sigma$ [-]
We_{crit}	critical Weber number [-]
x	spatial coordinate [m]
$y+$	dimensionless wall distance [-]
α	void fraction [-]
ε	turbulence energy dissipation rate [$m^2 s^{-3}$]
θ	contact angle [rad]
λ	thermal conductivity [W $m^{-1} K^{-1}$]
μ	viscosity [Pa s]
ν_t	turbulent kinematic viscosity [$m^2 s^{-1}$]
ρ	density [kg m^{-3}]
σ	surface tension [N m^{-1}]
τ_{BI}	bubble-induced turbulence timescale [s]
τ_{br}	break-up timescale [s]

Subscripts

c	continuous phase
d	dispersed phase
i	inner
in	inlet
l	liquid
o	outer
r	relative
sat	saturation
v	vapour
w	wall

References

[1] L.S. Tong, G.F. Hewitt, Overall view point of flow boiling CHF mechanisms, ASME paper 72-HT-54, 1972.

[2] J.G. Collier, J.R. Thome, Convective boiling and condensation, 3rd ed., Oxford University Press, Oxford, 1994.

[3] D. Bestion, Applicability of two-phase CFD to nuclear reactor thermalhydraulics and elaboration of Best Practice Guidelines, Nucl. Eng. Des. 253 (2012) 311-321.

[4] G. Yadigaroglu, CMFD and the critical-heat-flux grand challenge in nuclear thermal-hydraulics – A letter to the editor of this special issue, Int. J. Multhiphase Flow 67 (2014) 3-12.

[5] N. Kurul, M.Z. Podowski, Multidimensional effects in forced convection subcooled boiling, Proc. 9th International Heat Transfer Conference, Jerusalem, Israel, 1990.

[6] W. Yao, C. Morel, Volumetric interfacial area prediction in upward bubbly two-phase flow, Int. J. Heat Mass Tran. 47 (2004) 307-328.

[7] G.H. Yeoh, J.Y. Tu, Two-fluid and population balance models for subcooled boiling flow, Appl. Math. Model. 30 (2006) 1370-1391.

[8] B. Končar, M. Matkovic, Simulation of turbulent boiling flow in a vertical rectangular channel with one heated wall, Nucl. Eng. Des 245 (2012) 131-139.

[9] B.J. Yun, A. Splawski, S. Lo, C.H. Song, Prediction of a subcooled boiling flow with advanced two-phase flow models, Nucl. Eng. Des. 253 (2012) 351-359.

[10] E. Krepper, R. Rzehak, C. Lifante, T. Frank, CFD for subcooled flow boiling: Coupling wall boiling and population balance models, Nucl. Eng. Des. 255 (2013) 330-346.

[11] A. Tentner, P. Vegendla, A. Obabko, A. Tomboulides, P. Fischer, O. Marin, E. Merzari, Modeling of two phase flow in a BWR fuel assembly with a highly-scalable CFD code, 16th International Topical Meeting on Nuclear Reactor Thermal Hydraulics, Chicago, USA, 2015.

[12] R. Thakrar, J. Murallidharan, S.P. Walker, Simulations of high-pressure subcooled boiling flows in rectangular channels, 16th International Topical Meeting on Nuclear Reactor Thermal Hydraulics, Chicago, USA, 2015.

[13] T.H. Lee, G.C. Park, D.J. Lee, Local flow characteristics of subcooled boiling flow of water in a vertical concentric annulus, Int. J. Multiphase Flow 28 (2002) 1351-1368.

[14] R.P. Roy, S. Kang, J.A. Zarate, A. Laporta, Turbulent subcooled boiling flow – Experiments and simulations, J. Heat Tran.-T. ASME 124 (2002) 73-93.

[15] E. Krepper, B. Končar, Y. Egorov, CFD modelling and subcooled boiling – Concept, validation and application to fuel assembly design, Nucl. Eng. Des. 237 (2007) 716-731.

[16] E. Krepper, R. Rzehak, CFD for subcooled flow boiling: Simulation of DEBORA experiments, Nucl. Eng. Des. 241 (2011) 3851-3866.

[17] S. Lo, Application of the MUSIG model to bubbly flows, AEAT-1096, AEA Technology, 1996.

940 [18] C. Morel, J.M. Laviéville, Modeling of multisize bubbly flow and application to the
941 simulation of boiling flows with the Neptune_CFD code, Science and Technology of
942 Nuclear Installation Vol. 2009, Article ID 953527.
943 [19] S. Lo, P. Rao, Modelling of droplet breakup and coalescence in an oil-water pipeline,
944 paper 136, 6th International Conference on Multiphase Flow, Leipzig, Germany, 2007.
945 [20] S. Lo, D. Zhang, Modelling of break-up and coalescence in bubbly two-phase flows, J.
946 Comput. Multiphase Flow 1 (2009) 23-38.
947 [21] R.P. Roy, V. Velidandla, S.P. Kalra, Velocity field in turbulent subcooled boiling flow,
948 J. Heat Tran.-T. ASME 119 (1997) 754-766.
949 [22] G. Garnier, E. Manon, G. Cubizolles, Local measurements on flow boiling of refrigerant
950 12 in a vertical tube, Multiphase Sci. Technol. 13 (2001) 1-111.
951 [23] C.E. Estrada-Perez, Y.A. Hassan, PTV experiments of subcooled boiling flow through a
952 vertical rectangular channel, Int. J. Multiphase Flow 36 (2010) 691-706.
953 [24] G.G. Bartolomej, V.M. Chanturiya, Experimental study of true void fraction when
954 boiling subcooled water in vertical tubes, Therm. Eng. 14 (1967) 123-128.
955 [25] G.G. Bartolomej, V.G. Brantov, Y.S. Molochnikov, Y.V. Kharitonov, V.A. Solodkij,
956 G.N. Batashova, V.N. Mikhajlov, An experimental investigation of the true volumetric
957 vapour content with subcooled boiling tubes, Therm. Eng. 29 (1982), 20-22.
958 [26] C.C.St. Pierre, S.G. Bankoff, Vapor volume profiles in developing two-phase flow, Int. J.
959 Heat Mass Tran. 10 (1967) 237-249.
960 [27] S.C.P. Cheung, S. Vahaji, G.H. Yeoh, J.Y. Tu, Modeling subcooled flow boiling in
961 vertical channels at low pressure – Part1: Assessment of empirical correlations, Int. J.
962 Heat Mass Tran. 75 (2014) 736-753.
963 [28] R. Thakrar, J.S. Murallidharan, S.P. Walker, An evaluation of the RPI model for the
964 prediction of the wall heat flux partitioning in subcooled boiling flows, 22nd International
965 Conference on Nuclear Engineering, Prague, Czech Republic, 2014.
966 [29] M. Lemmert, J.M. Chawla, Influence of flow velocity on surface boiling heat transfer
967 coefficient, in: E. Hahne, U. Grigull (Eds.), Heat transfer in boiling, Academic Press and
968 Hemisphere, New York, 1977, pp. 237-247.
969 [30] T. Hibiki, M. Ishii, Active nucleation site density in boiling systems, Int. J. Heat Mass
970 Tran. 46 (2003) 2587-2601.
971 [31] V.I. Tolubinsky, D.M. Kostanchuk, Vapour bubbles growth rate and heat transfer
972 intensity at subcooled water boiling, Proc. 4th International Heat Transfer Conference,
973 Paris, France, 1970.

[32] G. Kocamustfaogullari, Pressure dependence of bubble departure diameter for water, Int. Commun. Heat Mass Tran. 10 (1983) 501-509.
[33] R. Cole, A photographic study of pool boiling in the region of the critical heat flux, AIChE J. 6 (1960) 533-538.
[34] S.C.P. Cheung, S. Vahaji, G.H. Yeoh, J.Y. Tu, Modeling subcooled flow boiling in vertical channels at low pressure – Part2: Evaluation of mechanistic approach, Int. J. Heat Mass Tran. 75 (2014) 754-768.
[35] D. Lucas, E. Krepper, R. Rzehak, Y. Liao, T. Ma, T. Ziegenhein, Status and challenges of CFD-modelling for poly-disperse bubbly flows, 16th International Topical Meeting on Nuclear Reactor Thermal Hydraulics, Chicago, USA, 2015.
[36] D. Lucas, R. Rzehak, E. Krepper, T. Ziegenhein, Y. Liao, S. Kriebitzsch, P. Apanasevich, A strategy for the qualification of multi-fluid approaches for nuclear reactor safety, Nucl. Eng. Des. 299 (2016) 2-11.
[37] S. Mimouni, F. Archambeau, M. Boucker, J. Laviéville, C. Morel, A second order turbulence model based on a Reynolds stress approach for two-phase boiling flow. Part 1: Application to the ASU-annular channel case, Nucl. Eng. Des. 240 (2010) 2233-2243.
[38] S. Mimouni, J. Laviéville, N. Seiler, P. Ruyer, Combined evaluation of second order turbulence model and polydispersion model for two-phase boiling flow and application to fuel assembly analysis, Nucl. Eng. Des. 241 (2011) 4523-4536.
[39] D.A. Drew, S.L. Passman, Theory of multicomponent fluids, Springer, New York, 1998.
[40] M. Ishii, T. Hibiki, Thermo-fluid dynamics of two-phase flow, Springer, New York, 2006.
[41] D. Lucas, E. Krepper, H.-M. Prasser, Use of models for lift, wall and turbulent dispersion forces acting on bubbles for poly-disperse flows, Chem. Eng. Sci. 62 (2007) 4146-4157.
[42] Y. Liao, R. Rzehak, D. Lucas, E. Krepper, Baseline closure model for dispersed bubbly flow: Bubble coalescence and breakup, Chem. Eng. Sci. 122 (2015) 336-349.
[43] A. Tomiyama, I. Kataoka, I. Zun, T. Sakaguchi, Drag coefficients of single bubbles under normal and micro gravity conditions, JSME Int. J. B - Fluid T. 41 (1998) 472-479.
[44] T.R. Auton, The lift force on a spherical body in a rotational flow, J. Fluid Mech. 183 (1987) 199-218.
[45] A. Tomiyama, H. Tamai, I. Zun, S. Hosokawa, Transverse migration of single bubbles in simple shear flows, Chem. Eng. Sci. 57 (2002) 1849-1858.
[46] S.P. Antal, R.T. Lahey Jr, J.E. Flaherty, Analysis of phase distribution in fully developed laminar bubbly two-phase flow, Int. J. Multiphase Flow 17 (1991) 635-652.

[47] M. Ullrich, R. Maduta, S Jakirlic, Turbulent bubbly flow in a vertical pipe computed by an eddy-resolving Reynolds stress model, Proc. 10th International ERCOFTAC Symposium on Engineering Turbulence Modelling and Measurements, Marbella, Spain, 2014.

[48] M. Colombo, M. Fairweather, Multiphase turbulence in bubbly flows: RANS simulations, Int. J. Multiphase Flow 77 (2015) 222-243.

[49] A.D. Burns, T. Frank, I. Hamill, J.M. Shi, The Favre averaged drag model for turbulent dispersion in Eulerian multi-phase flows, 5th International Conference on Multiphase Flow, Yokohama, Japan, 2004.

[50] C.G. Speziale, S. Sarkar, T.B. Gatski, Modelling the pressure-strain correlation of turbulence: an invariant dynamical system approach, J. Fluid Mech. 227 (1991) 245-272.

[51] Cd-Adapco, STAR-CCM+® Version 10.04 User Guide, 2015.

[52] B.J. Daly, F.H. Harlow, Transport equations of turbulence, Phys. Fluids 13 (1970) 2634-2649.

[53] A.D. Gosman, C. Lekakou, S. Politis, R.I. Issa, M.K. Looney, Multidimensional modeling ot turbulent two-phase flows in stirred vessels, AIChE J. 38 (1992) 1946-1956.

[54] A.A. Troshko, Y.A. Hassan, A two-equation turbulence model of turbulent bubbly flows, Int. J. Multiphase Flow 27 (2001) 1965-2000.

[55] A. Behzadi, R.I. Issa, H. Rusche, Modelling of dispersed bubble and droplet flow at high phase fractions, Chem. Eng. Sci. 59 (2004) 759-770.

[56] S.K. Wang, S.J. Lee, O.C. Jones Jr, R.T. Lahey Jr, 3-D turbulence structure and phase distribution measurements in bubbly two-phase flows, Int. J. Multiphase Flow 13 (1987) 327-343.

[57] M. Lance, J. Bataille, Turbulence in the liquid phase of a uniform bubbly air-water flow, J. Fluid Mech. 222 (1991) 95-118.

[58] M.E. Shawkat, C.Y. Ching, M. Shoukri, On the liquid turbulence energy spectra in two-phase bubbly flow in a large diameter pipe, Int. J. Multiphase Flow 33 (2007) 300-316.

[59] I. Kataoka, A. Serizawa, Basic equations of turbulence in gas-liquid two-phase flow, Int. J. Multiphase Flow 15 (1989) 843-855.

[60] R. Rzehak, E. Krepper, CFD modeling of bubble-induced turbulence, Int. J. Multiphase Flow 55 (2013) 138-155.

[61] M. Colombo, M. Fairweather, S. Lo, A. Splawski, Multiphase RANS simulation of turbulent bubbly flows, 16th International Topical Meeting on Nuclear Reactor Thermal Hydraulics, Chicago, USA, 2015.

[62] H. Luo, H.F. Svendsen, Theoretical model for drop and bubble breakup in turbulent dispersions, AIChE J. 42 (1996) 1225-1233.

[63] V.H. Del Valle, D.B.R. Kenning, Subcooled flow boiling at high heat flux, Int. J. Heat Mass Tran. 28 (1985) 1907-1920.

[64] W.E. Ranz, W.R. Marshall, Evaporation from drops, Chem. Eng. Prog. 48 (1952) 141-146.

[65] M. Colombo, M. Fairweather, RANS simulation of bubble coalescence and break-up in bubbly two-phase flows, Chem. Eng. Sci. 146 (2016) 207-225.

[66] H.C. Unal, Maximum bubble diameter, maximum bubble-growth time and bubble-growth rate during the subcooled nucleate flow boiling of water up to 17.72 MN/m^2, Int. J. Heat Mass Tran. 19 (1976) 643-649.

[67] J.F. Klausner, R. Mei, D.M. Bernhard, L.Z. Zeng, Vapor bubble departure in forced convection boiling, Int. J. Heat Mass Tran. 36 (1993) 651-662.

[68] L.Z. Zeng, J.F. Klausner, R. Mei, A unified model for the prediction of bubble detachment diameters in boiling systems – II. Flow boiling, Int. J. Heat Mass Tran. 36 (1993) 2271-2279.

[69] B. Končar, B. Mavko, Wall function approach for boiling two-phase flows, Nucl. Eng. Des. 240 (2010) 3910-3918.